Aus dem Institut für Physiologie und Pathophysiologie
-Geschäftsführender Direktor: Prof. Dr. Dr. Daut-
Des Fachbereichs Medizin der Philipps-Universität Marburg

Analysen und Modellierung multimodaler Interaktionen der renalen Autoregulation

Analysis and modelling of multimodal interactions in renal autoregulation

Inaugural-Dissertation zur Erlangung des Doktorgrades der gesamten Humanbiologie
Dem Fachbereich Medizin der Philipps-Universität Marburg
Vorgelegt von

Olga Sosnovtseva
aus Koselsk

Marburg/Lahn
2010

Angenommen vom Fachbereich Medizin der Philipps-Universität Marburg am: 15.04.10

Gedruckt mit Genehmigung des Fachbereichs

Dekan: Prof. Dr. Rothmund
Referent: PD. Dr. Braun
1. Korreferent: Prof. Dr. Dahlke

Contents

Zusammenfassung

Die Nieren sind wesentlich an der Regulierung des Wasser- und Elektrolyt-Haushalts beteiligt, und haben damit auch eine wichtige Funktion für die Langzeit-Regulation des Blutdrucks, mit zusätzlicher Kontrolle durch das Renin-Angiotensin System. Störungen der Nierenfunktion können zu Hypertonie führen, einer häufigen Krankheit in modernen Gesellschaften.

Die Nieren selbst sorgen für eine optimale Funktion, indem sie sich vor Kurzzeit-Schwankungen des Blutdruckes schützen. Auf der Ebene des Nephrons, der kleinsten Funktionseinheit der Niere, werden Nierendruck und Strömung durch zwei Mechanismen kontrolliert: durch das tubuloglomeruläre Feedback, das den einströmenden Blutfluss in Abhängigkeit von der NaCl-Konzentration in der tubulären Flüssigkeit nahe des Endpunktes der Henle-Schleife (macula densa) regelt, und durch einen myogenen Mechanismus, bei dem die afferente Arteriole ihren Durchmesser dem transmuralen Druck anpasst. Es ist experimentell bewiesen, dass beide Rückkopplungs-Mechanismen zu Oszillationen führen.

In der vorliegenden Studie werden durch die Analyse experimenteller Daten des tubulären Druck und des Blutflusses in den Arteriolen in Verbindung mit Computer-Modellen der Autoregulation folgende Fragen bearbeitet: (i) Können Wechselbeziehungen zwischen diesen beiden Mechanismen der renalen Selbstregulierung erkannt und charakterisiert werden? (ii) Führt die Wechselwirkung zwischen benachbarten Nephronen zu synchronisiertem Verhalten? (iii) Lassen sich im Vergleich normo- und hypertensiver Ratten Unterschiede der Autoregulation oder Synchronisation erkennen?

Die Analyse der experimentellen Zeitreihen ergab, dass die myogenen Oszillationen sowohl einer Amplituden als auch Frequenzmodulation unterliegen, was auf einen modulierenden Einfluss des tubulo-glomulären Rückkopplungskreises hindeutet. Es zeigte sich, dass die Wechselwirkung zwischen den beiden Oszillatoren der renalen Autoregulierung bei spontan hypertensiven Ratten signifikant stärker als bei normotensiven Ratten ausgeprägt ist.

Der Synchronisationsgrad benachbarter Nephronen wurde durch Bestim-

mung von Frequenz und Phasenentrainment erfasst. Eine statistische Analyse zeigte, dass die Synchronisation zwischen den renalen Autoregulierungs-Mechanismen in hyptertensiven Ratten reduziert ist. Mit mehr als 80%er Wahrscheinlichkeit zeigten normotensive Ratten eine vollständige Synchronisation benachbarter Nephronen, was bedeutet, dass beide Prozesse der Autoregulierung synchron verlaufen. Bei hypertensiven Ratten war die Wahrscheinlichkeit vollständiger Synchronisation war auf die Hälfte reduziert (40%). Dahingegen fand sich eine doppelt so große Wahrscheinlichkeit für partielle Synchronisation - einem Zustand, bei dem nur einer der beiden Rückkopplungskreise, entweder der tubuloglomeruläre oder der myogene, synchronisiert ist. Außerdem dauern bei spontan hypertensiven Ratten die Phasen der Synchronisation nur ein drittel oder halb so lange wie bei normotensiven Ratten.

Diese experimentellen Befunde konnten in Computer-Simulationen reproduziert werden, wobei Oberflächen-Nephronen über eine hämodynamische und eine vaskulär vermittelte Kopplung verknüpft sind. Sowohl Experiment als auch Modell lassen vermuten, dass der Mangel an Synchronisation für die Entstehung irregulärer Dynamik in den Tubuli von Ratten mit experimenteller Hypertonie verantwortlich sein kann.

Dieses Computer-Modell wurde durch die Einbeziehung tiefliegender Nephronen erweitert, an denen entsprechende experimentelle Messungen bislang nicht möglich sind. Unter Berücksichtigung der aktuell verfügbaren anatomischen und physiologischen Informationen, zeigen die Computer Simulationen zunehmende Unregelmäßigkeiten im Zusammenspiel der Nephronen wenn der arterielle Druck zunimmt oder die Wechselwirkung zwischen den Nephronen größer wird. Allerdings lassen sich bei physiologischen Parameterwerten die tiefliegenden Nephronen nicht mit den Oberflächen-Nephronen synchronisieren, obwohl beide ber ihre Blutverssorgung gekoppelt sind.

Summary

By maintaining the volume and composition of the body fluids within narrow bounds and by producing a set of hormones that affect the blood vessels, the kidneys provide important long-term regulation of the blood pressure. Disturbances of kidney function can cause hypertension, a prevalent disease in modern societies.

The kidneys protect their own function against short-term variations in the blood pressure. At the level of the individual functional unit (the nephron), pressure and flow control involves two different mechanisms: the tubuloglomerular feedback, which regulates the incoming blood flow in response to variations of the NaCl concentration of the tubular fluid near the terminal point of the loop of Henle (macula densa), and a myogenic mechanism by which the afferent arteriole regulates its diameter in response to variations in its transmural pressure. Experimentally, both of these mechanisms are found to produce oscillations.

In the present study, analysis of experimental data of the tubular pressure and arteriole blood flow in combination with mechanism-based modelling has been used to answer the following questions: (i) How to reveal and characterize interactions between the two mechanisms of renal autoregulation? (ii) To what extend does nephron-to-nephron communication lead to cooperative behaviour? and (iii) How do intra- and inter-nephron interactions differ in normotensive and hypertensive rats?

Analysis of experimental data revealed the presence of amplitude and frequency modulation, i.e. the regulation is provided not only by a change in the diameters of the active parts of the vessels, but also by an adjustment of the frequency of the myogenic oscillations. Interaction between the two mechanisms of renal autoregulation was found to be significantly stronger in spontaneously hypertensive rats than in normotensive rats.

Synchronization phenomena in neighbouring nephrons were evaluated by measuring both frequency and phase entrainment. Statistical analysis showed that synchronization among mechanisms of renal autoregulation is reduced in hypertensive rats. With a probability exceeding 80%, normotensive rats demon-

strated full entrainment in neighbouring nephrons where the oscillatory modes associated with two mechanisms of autoregulation were synchronized. Hypertensive rats displayed about half the probability of full synchronization and about twice the probability of partial synchronization, i.e. a state where neighbouring nephrons synchronize their slow tubuloglomerular feedback dynamics, while the fast myogenic dynamics remain desynchronized, or vice versa. Spontaneously hypertensive rats generally remained in synchrony for only 1/3 to 1/2 as long as the normotensive ones.

Numerical simulations with a model of superficial nephrons connected via a flow mediated hemodynamic coupling and a vascular propagated coupling reproduced the experimentally observed patterns of behaviour. Lack of synchronization may be responsible for the development of irregular dynamics in the tubules of rats with experimental hypertension.

The model has been extended by including deep nephrons for which it has not yet been possible to perform similar experimental measurements. Using available anatomical and physiological information we constructed a model of an nephron-vascular ensemble including superficial as well as deep nephrons with different length of loop of Henle. The computer simulation suggested that irregular dynamics of nephron ensemble increases at higher arterial pressures and values of the coupling strength. The model showed that, for physiologically reasonable parameter values, the deep nephrons do not synchronize with the superficial nephrons even though they are coupled via the same blood supply.

Chapter 1

Introduction

The kidney regulates the incoming blood flow at the level of each nephron through a combination of regulatory mechanisms. The balance of their contributions are an important determinant for the kinetics and function of the overall autoregulation. The overall speed of renal blood flow regulation is crucial because the kidney vasculature is continuously challenged by fluctuations of pressure over a broad range of frequencies from rhythmic processes of seconds and minutes (di Rienzo et al., 1989) to hours and days (Blinowska and Marsh, 1985). Since autoregulation determines the amount of pressure fluctuations reaching the glomerulus, peritubular capillaries, and the medullary circulation, its function is important for filtration, reabsorption and hypertensive renal damage.

Present research has been performed to address several questions:

- How to reveal and characterize interaction between renal regulatory mechanisms?
- How does nephron-to-nephron communication lead to cooperative behavior?
- What are the possibilities and limitations of modeling approach?

1.1 Systems biology approach

Systems Biology is a rapidly developing area of research that aims to explain the complex cellular and physiological phenomena of living organisms in terms of the underlying chemical and physical processes and the involved feedback regulations on different time- and space-scales (Marcus, 2008). Understanding of the system behavior is based on the description of the functional interactions between the key components of cells, tissues and organs, as well as of how these interactions change at states of disease. The approach is based on a close integration of experiments and theory and involves new methods for analysis of the large amount of biological data provided by the rapidly developing experimental techniques (Fig. 1.1).

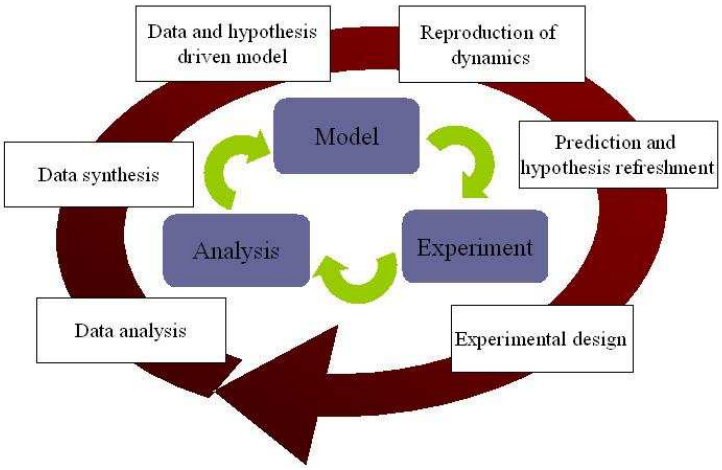

Figure 1.1: Systems biology approach combines new experimental techniques with mechanism-based modeling and advanced methods of data analysis.

Systems Biology is a scientific approach that seeks to understand how all the individual components of a biological system interact in time and space to determine the functioning of the system (Bertau et al., 2008). This involves description of

- The structure of a biological system, i.e. the significant physiological

components and their structural relationships at the appropriate spatial scale;

- The dynamical behavior of the system under different conditions and external perturbations;
- The mechanisms that control the states and behavior of the system;
- The causes of system changes in connection with various diseases and the methods by which such changes can be counteracted or compensated.

The concept of homeostasis (Cannon, 1929), i.e. the ability of the body to maintain a nearly constant internal milieu despite of changes in the external conditions, plays an essential role in the description of physiological control systems. It is sometimes assumed that homeostasis implies that the physiological variables are kept near a stable steady state by means of an effective feedback regulation. While this may be the case in certain situations, biological systems in general should be considered as open dissipative systems that are maintained under far-from-equilibrium conditions (Nicolis and Prigogine,1977). Regular and irregular oscillations associated with various forms of instability are common features of behavior that can be observed during normal functioning or arise in connection with particular states of disease (Glass and Mackey, 1988).

Living systems often generate signals that reflect the coexistence of rhythmic components originating in different mechanisms. Besides the heart beat, analysis of blood pressure data, for instance, are likely to reveal components produced by both the respiratory cycle and the vasomotoric activity of small arteries and arterioles (Hoffman et al., 1990; Holstein-Rathlou et al. 1995). The presence of such multimode dynamics is well-documented for physiological control systems at the cellular or subcellular level (e.g., the bursting activity of pancreatic β-cells (Ashcroft and Rorsman, 1989; Goldbeter, 1996) and of certain nerve cells (Braun et al. 1994; Wang and Rinzel, 1995) and the systemic level (e.g., the coexistence of a 24 h circadian rhythm and a 2-4 h ultradian rhythm in hormone secretion (Leng, 1988)).

Interaction between coexisting rhythms can lead to a variety of interesting nonlinear dynamic phenomena, with synchronization representing the most prominent example. Experimental and/or numerical investigations of synchronization have been performed for many different physiological systems, including, for instance, the cardio-respiratory system (Schäfer et al., 1998) and small ensembles of nerve cells (Kopell et al., 2000). However, even when synchronization does not occur, the mode-to-mode interaction may reveal itself in the form of modulation. The instantaneous amplitude or frequency of one mode may be modulated by the presence of the other (Mosekilde, 1996).

Physiological processes are often highly nonstationary. Part of this nonstationarity may be ascribed to changing environmental conditions or to interactions with other regulatory processes. It is known, however, that the degree of nonstationarity can differ between states of health and disease (Wolf et al., 1978). If the properties of the experimental data display essential variations over short time intervals, one has to apply specialized tools such as wavelet analysis (Grossman and Morlet, 1984; Daubechies, 1992; Kaiser, 1994) or detrended fluctuation analysis (Peng et al., 1995).

1.2 Renal physiology

1.2.1 Kidney function

The kidneys serve multiple functions including: regulating water and electrolyte balance, excretion of metabolic products, secretion of hormones and regulation of arterial pressure. The kidneys play an important role in maintaining a proper environment for the cells in the body. By regulating the excretion of water, salts and metabolic end products, the kidneys control the plasma osmolality (i.e., the total concentration of ions and molecules in the blood), the extracellular fluid volume, and the proportions of various blood solutes (Alpern and Heber, 2008).

The interaction between the kidneys and the cardiovascular system is complex. The kidneys provide important long-term regulation of the cardiovascular system by maintaining the volume and composition of the body fluids within

narrow bounds and by producing a set of hormones that affect blood vessels within the kidneys and elsewhere in the body. Disruption of kidney function can cause hypertension, a prevalent disease in modern societies. The kidneys are also perfused with blood and are thus exposed to all of the fluctuations present in the cardiovascular system. There are two major periodicites in the blood pressure: one at the frequency of the heart rate and the other with the period of 24 h. Over the intermediate bandwidth between these periodicities the blood pressure displays a $1/f$ pattern. The $1/f$ fluctuations are caused by the independent actions of arterioles in all organs of the body, with contractions of large muscles making particularly strong contributions, and they present a specific challenge to the kidneys as they serve to regulate the body fluids. The kidneys protect their own function against short-term variations in the blood pressure. The process of autoregulation takes place at the level of individual nephron.

1.2.2 Nephron as functional unit

Figure 1.2 (left) illustrates the main structure of the nephron. Blood enters the system through the afferent arteriole, a short vessel that is capable of regulating the blood flow by varying its diameter. At the glomerulus the blood passes a system of parallel capillary loops, where $25-35\%$ of the water together with blood constituents with low molecular weight is filtered out into the proximal tubule. Blood cells and proteins are retained, and the filtration process saturates when the colloid osmotic pressure balances the hydrostatic pressure difference between the blood and the filtrate in the tubule. The blood leaves the glomerulus through the efferent arteriole to pass through a new capillary bed and out into the venous system. In the second capillary bed, which embraces the tubule, a nearly constant fraction of the filtrate is reabsorbed.

The other component of a nephron is a hollow tube with a membrane wall formed by a single layer of highly specialized epithelial cells. With its various sections: the proximal tubule, the loop of Henle, the distal tubule, and the collecting duct, the total length of the nephron is approximately 2 cm. The inner

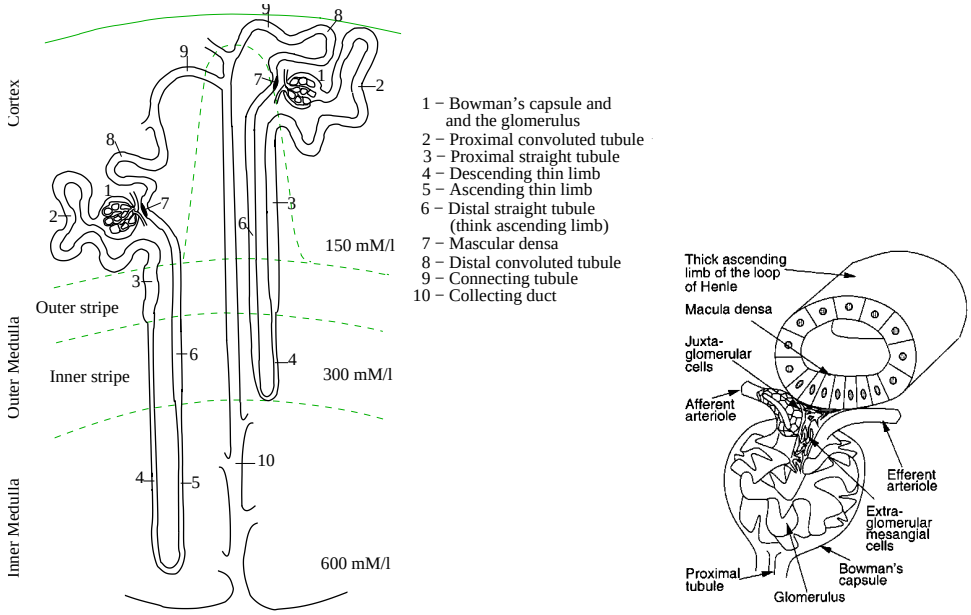

Figure 1.2: Schematic figure of (left) the major components of superficial (cortical) and deep (juxtamedullary) nephrons showing afferent and efferent arteriole, glomerulus, proximal tubule, loop of Henle and distal tubular and (right) the renal corpuscle with different parts of the juxtaglomerulus apparatus.

diameter, however, is only about 20 μm. The proximal tubule is located within the outer layer of the kidney, the cortex, and is hence accessible for pressure measurements by means of glass micropipettes. From the proximal tubule the nephron traverses down through the renal medulla, forming the descending and ascending limb of the loop of Henle. When reentering the cortex, the ascending limb changes tissue type to become the distal tubule. The interesting anatomical feature that the terminal part of the ascending limb passes immediately by the afferent arteriole of the same nephron forms the basis for the tubuloglomerular feedback. At the point of contact, specialized tubular cells – macula densa cells – monitor the composition of the tubular fluid and produce a signal that acts on the smooth muscle cells in the wall of the afferent arteriole (Fig. 1.2, right).

Except that there are no large molecules, the composition of the ultrafiltrate in the proximal tubule is like that of the blood plasma. Without changing the composition much, the proximal tubule reabsorbs approximately two-thirds of the water and salts. As the filtrate flows into the descending limb of the loop of

Henle, the concentration of NaCl in the interstitial fluid surrounding the tubule increases significantly, and osmotic processes cause a reabsorption of water. At the same time salts and metabolic end products are secreted into the tubular fluid. The ascending limb, on the other hand, is practically impermeable to water, and its epithelial cells contain molecular pumps that transport sodium and chloride from the tubular fluid into the surrounding interstitium. In this way the NaCl concentration of the tubular fluid is again reduced. Near the terminal part of the loop of Henle, the macula densa cells monitor the NaCl concentration of the tubular fluid and produce a feedback signal to the afferent arteriole.

1.2.3 Mechanisms of autoregulation

The tubuloglomerular feedback

Tubuloglomerular feedback (TGF) is a regulating mechanism specific to the kidney that leads to vasoconstriction of the afferent arteriole in response to an increase of the luminal concentration of NaCl at the macular densa in the early distal tubule (Schnermann et al., 1998). Because of salt reabsorption from the ascending part of the loop of Henle is an active and more rate limited process than the passive diffusion of water out of descending limb, the concentration of NaCl reaching the macula densa is dependent on the rate of tubular flow with larger flow resulting in a higher distal tubular concentration. An increase in arterial pressure will enhance tubular flow due to enhanced glomarular filtration and reduced proximal tubular reabsorption. This will raise the NaCl concentration at the macular densa and cause afferent arteriolar vasocontriction, providing restoration of filtration and autoregulation of renal blood flow. The TGF mechanism produces a negative feedback control that regulates the nephronal blood flow.

A large number of studies have provided an insight in the signalling pathways of the tubuloglomerular feedback as summarized in many comprehensive reviews (Thomson and Blantz, 1988; Bell et al., 2003; Schnermann and Levine, 2003). There is an agreement that the initial absorption of NaCl through furosemide-

sensitive Na^+-K^+-$2Cl^-$ cotransport results in release of ATP from macular densa cells. Released ATP can directly activates ATP-specific purino-receptors of the P2X1-type located on the afferent arteriole or can be converted to adenosine which then acts on A1 adenosine receptors of the P1-group of purinoreceptors.

Leyssac and Baumbach were the first to describe the presence of self-sustained oscillations in the proximal hydrostatic pressure in anesthetized rats (Leyssac and Baumbach, 1983). The oscillations had a period of about 30 sec (0.033 Hz). The same oscillations have been found in renal blood flow in anesthetized (Holstein-Rathlou et al., 1991) and conscious rats (Pires et al., 2001). Similar oscillations were seen in conscious dogs at lower frequency of 0.025 Hz (Just et al., 1998). Several potential delays exist in the TGF system:

- Transmission of the signal through the tubular system from the glomerulus to the macula densa. Holstein-Rathlou and Marsh showed that oscillations in late proximal flow rate, early distal pressure, and early distal Cl^- activity are associated with the oscillations in proximal pressure (Holstein-Rathlou and Marsh, 1989). These different oscillating variables were not in phase with each other. Thus, early distal Cl^- activity lagged proximal pressure by 8-10.5 seconds;

- Transmission of the signal across the macula densa to the afferent arteriole and the time necessary for the afferent arteriole to contract in response to the signal originating at the macula densa. The signal transduction from the macula densa to the afferent arteriole in response to changes in tubular NaCl concentration shows a delay of 3 s followed by a rapid vasoconstriction over another 3 s, i.e. the entire response is completed within 5-6 s (Casellas and Moore, 1990).

While for normal rats the oscillations have the appearance of regular self-sustained oscillations, highly irregular oscillations are observed for spontaneously hypertensive rats (Holstein-Rathlou and Leyssac, 1986; Leyssac and Holstein-Rathlou, 1989). Normal rats made hypertensive by clipping one renal artery had similar aperiodic tubular oscillations in the unclipped kidney (Yip et al., 1991).

The most compelling evidence for a key role of the kidney in the pathogenesis of hypertension comes from renal cross transplantation studies (Rettig et al., 1989; Rettig et al., 1990). Rats from the F1 generation of Wistar Kyoto and stroke prone SHR have a blood pressure between that of the parental strains. Transplantation of a kidney from a donor SHR into a rat from this F1 generation leads to an increase in the arterial pressure of the recipient to the level in SHR. this was the case even if the kidney was taken from a donor SHR that had been on chronic antihypertensive treatment since birth, and therefore had a normal blood pressure up to the time when the kidney was removed. Since two different model of hypertension display similar dynamics one can suggest that a transition of the regulatory behavior to a chaotic state is a common feature of renal vascular control in the development of disease.

The myogenic response

The myogenic response is a function of smooth muscle to contract in response to external stretching force (Johnson, 1980). In the case of vascular smooth muscle cells, a rise in intraluminal pressure induces a vasocontriction, that reduces the diameter below the one at lower pressure. This causes an increased vascular resistance at higher pressure and allows for autoregulation of flow.

The signalling pathways underlying myogenic response have been studied extensively (Davis and Hill, 1999; Schubert and Mulvany, 1999). One of the early events following myogenic activation is depolarization of cell membrane which mechanisms are still unclear (mechano-sensitive ion channels, activation of integrin receptor, or stretch-induced activation of phospholipase C). Once initiated, the depolarization is lead to influx of Ca^{2+} through voltage-gated Ca^{2+} -channels. The main signalling pathway following the rise in Ca^{2+} involves calmodulin and myosin light chain phosphorylation that cause constrictor response.

The frequency of the vasomotor oscillations varies with the vascular bed under study. It is shown that there is inverse relation between the size of the vessel and the frequency of oscillations (Colantuoni et al., 1984). The oscillations in

the radius of afferent arteriole are less than 10 s (Casellas and Moore, 1990; Clausen et al., 1992; Loutzenhiser et al., 2002).

Interaction between the mechanisms

The balance of the mechanisms contributing to renal blood flow autoregulation is not only determined by the algebraic summation of their influence, but also by interactions between them. TGF system and vasomotor oscillator operate in different frequency band: 0.02-0.04 Hz and 0.1-0.25 Hz, respectively. Since both mechanisms act on the afferent arteriole to control its hemodynamic resistance, the activation of one of the mechanisms modifies the response of the other (Schnermann and Briggs, 1989; Moore and Casellas, 1990; Yip et al., 1993; Chon et al., 2005).

Besides TGF and myogenic oscillations the third slower mechanism has been detected (Wronski et al., 2003). The underlying cause of the third regulatory mechanism remains unclear; possibilities include ATP, ANG II, or a slow component of myogenic response (Just, 2007). These slower oscillation can modulate activity of TFG and myogenic oscillations (Pavlov et al., 2008). Other mechanisms, which, however, exert their action through modulation of myogenic response and TGF are pressure-dependent change of proximal tubular reabsorption, modulating influences of ANG II and nitric oxide (NO).

1.2.4 Nephron-vascular tree

Nephrons are arranged in a tree structure with the afferent arteriole branching off from a common interlobular artery (Casellas et al., 1994) (Fig. 1.3). This structure allows a change in the blood flow to one nephron to influence the blood flow to all the other nephrons in the tree. Interaction between adjacent nephrons can occur due to (i) vascularly propagated coupling mediated by electrochemical signals and muscular contractions that travel along the arteriolar wall (Holstein-Rathlou, 1987) and (ii) hemodynamic coupling by which an increased flow resistance in the afferent arteriole leading to one nephron forces a higher blood flow to the neighboring nephrons. Using anatomical criteria,

neighboring nephrons having a high likelihood of deriving their afferent arterioles from the same interlobular artery were identified (Holstein-Rathlou and Leyssac, 1986; Chen et al., 1995). In these nephrons 29 out of 33 pairs (i.e., 88 %) were found to have synchronized oscillations. In contrast, nephron pairs not fulfilling these criteria only showed synchronous oscillations in one case out of 23 investigated pairs (i.e., 4 %). This observation shows that synchronized oscillations are preferentially found in nephrons originating from the same interlobular artery.

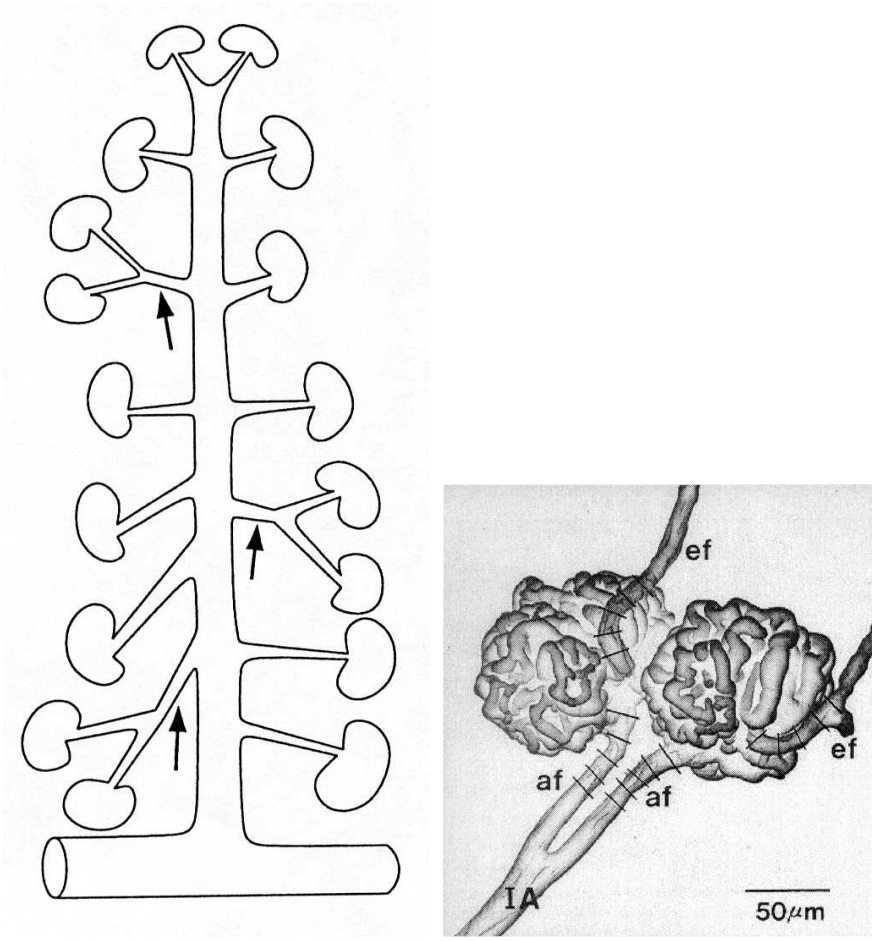

Figure 1.3: Left: Schematic presentation of interlobular artery with branching afferent arterioles. Right: Scanning electron microscope picture of the arteriolar system for two adjacent nephrons.

From measurements of signal strength in nephron-nephron communication it is estimated that the distance over which such signals can be effective is about

1.5 mm (Chen et al., 1995; Wagner et al., 1997). The renal cortex is about 2 mm deep in rats, and the cortical radial artery branches from the arcuate artery and penetrates toward the renal surface within the cortex. It is assumed, therefore, that the field of interacting nephrons consists of all those with afferent arterioles originating from a single cortical radial artery, which includes superficial (cortical) as well as deep (juxtamedullary) nephrons (Fig. 1.2). The number of nephrons originating from a single cortical radial artery varies somewhat; estimates are in the range of 20 - 40 (Casellas et al., 1997; Nordsletten et al., 2006).

So far, TGF oscillations and interaction between neighboring nephrons by virtue of the vascularly propagated signals have been studied experimentally only in cortical nephrons with tubular and vascular components on the surface of the kidney, but because the deeper nephrons have similar structures and regulatory mechanisms (Müller-Suur et al., 1983; Sjöquist et al., 1984), it is assumed that they, too, generate oscillations and are capable of interactions. Nephrons that lie deep within the kidney are longer than those on the surface, and because the TGF signal depends on flow rate dependent concentration changes reaching a tubular sensing site, one expects that the longer nephrons will oscillate more slowly than the shorter superficial ones. If all or most nephrons oscillate, and if they interact, synchronization and other forms of nonlinear interactions are to be expected among nephrons along the same cortical radial artery. But there is no experimental evidence yet.

1.3 Experimental background

Animal preparation. Experiments were performed in male Sprague-Dawley rats, 250–300 g body weight, and in 220–260 g body weight spontaneously hypertensive rats (SHR). Anesthesia was induced and maintained with 5% Halothane in a gas mixture containing 25% oxygen and 75% nitrogen. Maintenance anesthesia was administered through a tracheotomy tube by means of a respirator; blood pH was maintained between 7.35 and 7.45 and body temperature at 37 C. The left kidney was exposed.

Tubular pressure measurements. Experimental data were from previous studies (Yip et al., 1992). Simultaneous paired measurements of tubular pressure from two or three surface nephrons of the left kidney were made with the servo-nulling technique for up to 21 min (Fig. 1.4). Arterial blood pressure was measured in the left carotid artery with catheter filled with heparinized saline connected to pressure transducer.

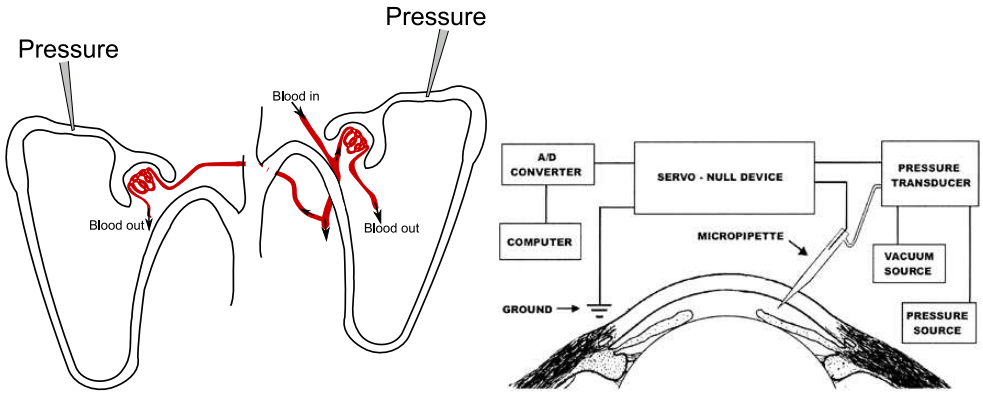

Figure 1.4: Left: Paired measurements of tubular pressure. Right: The servo-nulling micropipette system SNMS is an electrophysiologic, nonmanometric method of measuring pressure. It consists of an exploring micropipette, a ground reference, and a servo-null device.

The 13 normotensive rats had a mean arterial pressure of 111 ± 3 mm Hg, and the 18 SHR a mean arterial pressure of 144 ± 5 mm Hg. The normotensive rats provided 7 pairs of time series from nephrons that were not coupled, and 9 pairs of times series from coupled nephrons. The SHR gave 10 pairs of time series from uncoupled nephrons and 11 pairs time series from coupled nephrons. Vascular coupling here is defined as an origin of both nephrons of the pair from a single cortical radial artery, and was confirmed after each experiment by the preparation and examination of silicon casts of the renal vasculature.

Tubular pressure data was recorded through a low pass Butterworth filter with a cutoff frequency of 1.5 Hz. The data records, which varied in length from 240 to 1260 seconds were then digitized. The rate of digitization was varied, depending on the length of the recording, to produce records with 4096 points in each of the paired samples. The respiratory signal was removed with

a Kaiser-Bessel low-pass filter with a cutoff frequency of 0.5 Hz and attenuation of 50 dB. The calculations reported in this paper were performed on the output of the KaiserBessel filter.

Single nephron blood flow measurements. The experimental data were from the previous studies based on a laser-Doppler velocimetry device (Yip et al., 1993). The beam of a He-Ne laser was passed through an optical fiber to a GRIN-rod lens to reduce the beam diameter, and it was aimed at a single efferent arteriole on the surface of the kidney. The scattered light was collected with a second fiber, and Doppler frequency shifts were measured to determine relative velocity changes in blood flow. Details of the method are found in Ref (Smedley et al., 1993).

Chapter 2

Methods

2.1 Time-series analysis

Traditionally, analyses of biological time series have often been performed within the framework of the following ideology: It is supposed that segments of the experimental time series are approximately stationary, and that such segments can be studied by means of statistical techniques such as, for instance, correlation measures or Fourier analysis. This approach is obviously useful if the nonstationarity is associated only with the low-frequency region of the power spectrum relative to the rhythms of interest from the physiological point of view. Such nonstationarity is treated as a slow trend and may simply be filtered out from the data (Kantz and Schreiber, 2004). However, this situation is not always true for experimental recordings. As an example, besides a slow "floating" of the mean value, instantaneous frequencies of various rhythmic components can exhibit complex and irregular fluctuations, i.e. the nonstationarity may be associated with higher frequencies as well. Analysis of such time series using traditional statistical or spectral approaches can lead to misinterpretation of the obtained results. In particular, the coexistence of two peaks in the power spectrum of a physiological process can correspond to essentially different situations: There could be two independent modes or only a single mode whose instantaneous frequency changes in time from one value to another (Fig. 2.1). Such problems serve to underline the importance of developing new, more universal

tools to study the dynamics of complex systems.

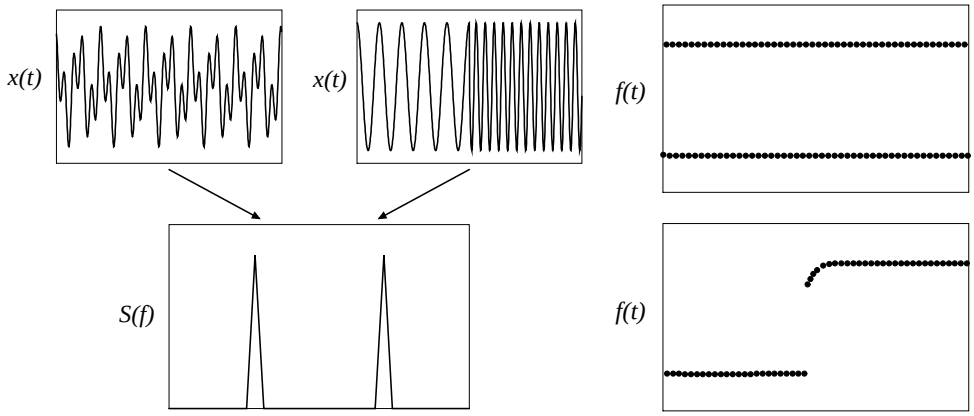

Figure 2.1: Classical spectral analysis can not distinguesh two different signals (left), while instantaneous frequncies obtained vie wavelet analisys can clearly seperate two cases (right).

From the viewpoint of possible applications, the attractiveness of a particular technique for signal processing depends on its generality, i.e. on the lack of restrictions on the signal properties. At the present, there are only few techniques that can cope with inhomogeneity and nonstationarity of biological time series. Among these the three most well-known are: (1) the construction of an analytical signal by means of a Hilbert transformation (Gabor, 1946), (2) the detrended fluctuation analysis (DFA) (Peng et al., 1995), and (3) the wavelet analysis (Grossman and Morlet, 1984; Daubechies, 1992).

The analytical signal approach allows us to introduce the notions of an instantaneous amplitude, phase and frequency for a random process. Thus we can analyze how these characteristics vary in time. This technique represents an effective tool for studying relations between signals, e.g. entrainment phenomena among biological rhythms. The DFA is a tool proposed to reveal features of long-range correlations. The main idea is to interpret experimental data as random walk and then analyze how this walk deviates from a local trend. Following Ref. (Peng et al., 1995), the characteristics of the DFA-method have a clear relation to the scaling exponents describing the behavior of the autocorrelation function or of the power spectrum. Thus, the DFA makes it possible to

perform spectral and correlation analyses of nonstationary processes. However, for such applications the wavelet-based multifractal analysis (Muzy et al., 1994) has a number of advantages, especially for short data series. For instance, the DFA-method requires a significantly larger length of the time series and it is not as effective in the analysis of correlation properties at small time scales.

2.1.1 Wavelet analysis

During the last decades, wavelet transformation has become an important tool in the spectral analysis of experimental data (Grossman and Morlet, 1984; Daubechies, 1992). Unlike the classical Fourier technique, wavelet transformation provides a means to follow the time evolution of particular spectral peaks. If we need to know only the periodicities that are revealed in a time series, then the classical methods can be successfully applied. However, if we are interested in the temporal dynamics of the rhythmic components, then the wavelets have a clear advantage. In this way, wavelet analysis has been widely applied in different fields (Meyer, 1992). One way to see the time-frequency resolution differences between the Fourier transform and the wavelet transform is to look at the basis function coverage of the time-frequency plane. Figure 2.2 shows simple comparison a windowed Fourier transform (WFT) and wavelet transform. The square wave window truncates the sine or cosine function to fit a window of a particular width. Because a single window is used for all frequencies in the WFT, the resolution of the analysis is the same at all locations in the time-frequency plane. An advantage of wavelet transforms is that the windows vary. In order to isolate signal discontinuities, one would like to have some very short basis functions. At the same time, in order to obtain detailed frequency analysis, one would like to have some very long basis functions. A way to achieve this is to have short high-frequency basis functions and long low-frequency ones. This happy medium is exactly what you get with wavelet transforms.

The wavelet transform of a signal x(t) involves its projection onto a set of soliton-like basis functions, obtained by rescaling and translating a “wavelet”

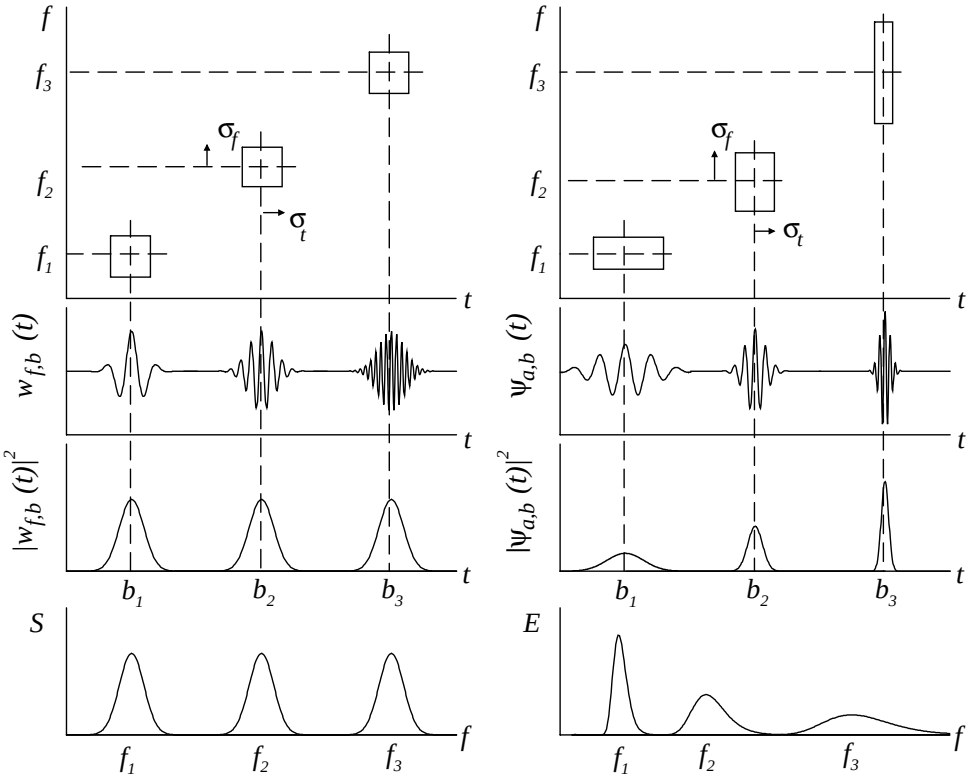

Figure 2.2: Frequency-time resolution of a window Fourier (left) and wavelet transform (right). For wavelet transform, with increasing frequency temporal resolution becomes better but spectral peaks becomes broader.

along the time axis:

$$W(a,b) = \frac{1}{\sqrt{a}} \int_{-\infty}^{\infty} x(t)\psi^* \left(\frac{t-b}{a} \right) dt, \tag{2.1}$$

where ψ is the wavelet basic function and the asterisk (*) denotes complex conjugation. $W(a,b)$ is referred to as the wavelet-transform of $x(t)$, which is a function of the time scaling and the translation parameters a and b, respectively. Besides being localized in both the time and frequency domains, the basic function should possess a few additional properties, such as zero mean, boundedness, and basis self-similarity (the latter means, for instance, that all wavelets constructed from a given basic function must have the same number of oscillations). The choice of ψ depends on the purpose of the analysis. Each wavelet function has its own features in the time and frequency domains. This provides us with the opportunity to reveal specific properties of a given biological signal. The wavelet-transform is often interpreted as a mathematical microscope whose optical characteristics are defined by the choice of the function ψ and the parameters a and b determine the magnification and the focusing point, respectively. In the spectral analysis of experimental time series one prefers complex wavelets, among which the most popular is the Morlet-wavelet whose simplified expression has the form:

$$\psi(\tau) = \pi^{-1/4} \exp(j2\pi f_0 \tau) \exp\left[-\frac{\tau^2}{2} \right]. \tag{2.2}$$

The value f_0 allows us to search for a compromise between the localization of the wavelet in the time and frequency domains (Fig. 2.3). The relation between time scale a and the central frequency for the function ψ is $f = f0/a$.

Besides the coefficients $W(a,b)$, the energy density of the signal $x(t)$ in the time scale plane can also be estimated: $E(a,b) \sim |W(a,b)|^2$. Following the definition used in Ref. (Kaiser, 1994), the coefficient of proportionality between $E(a,b)$ and $|W(a,b)|^2$ depends on both the scale and the shape of the "mother"

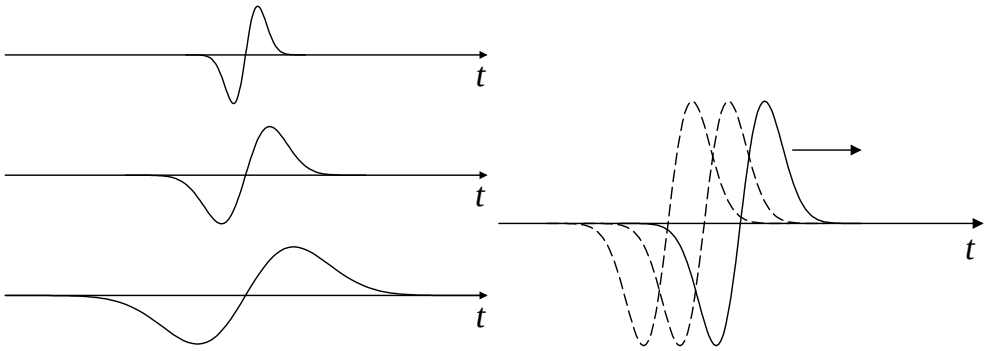

Figure 2.3: Mathematical transformation: (left) scale and (right) location.

wavelet although in some works the simpler expression $E(a,b) \sim |W(a,b)|^2$ is considered (Mallat, 1998). Note that the modula of the original wavelet coefficients $W(a,b)$ estimated from Eq. (2.1) do not correspond to actual amplitudes of the rhythmic components. To study amplitude variations, it is useful to slightly change the definition of the wavelet transform (Muzy et al., 1994) or to make corrections for the energy density $E(a,b)$. In the present study we will use the relation

$$E(a,b) = Ca^{-1} \mid W(a,b) \mid^2 \tag{2.3}$$

where C, a parameter that depends on the wavelet "mother" function, is kept constant. $E(a,b)$ represents a surface in 3-dimensional space whose sections at fixed time moments correspond to the local energy spectrum. To simplify the visualization of this surface, the dynamics of only the local maxima of $E(a,b)$ or $E(f,b)$, i.e., the time evolution of the spectral peaks will be considered. In this way, all frequency components being of physiological interest can be extracted from the original wavelet transform for further analysis of their properties.

Figures 2.4(a-d) illustrate the ability of the wavelet approach to detect and follow changes in the instantaneous frequency of a signal. Each figure has two panels. The top panel displays the test signal to be analysed, and the lower panel shows the detected frequency (or frequencies). The top panel of Fig. 2.4a

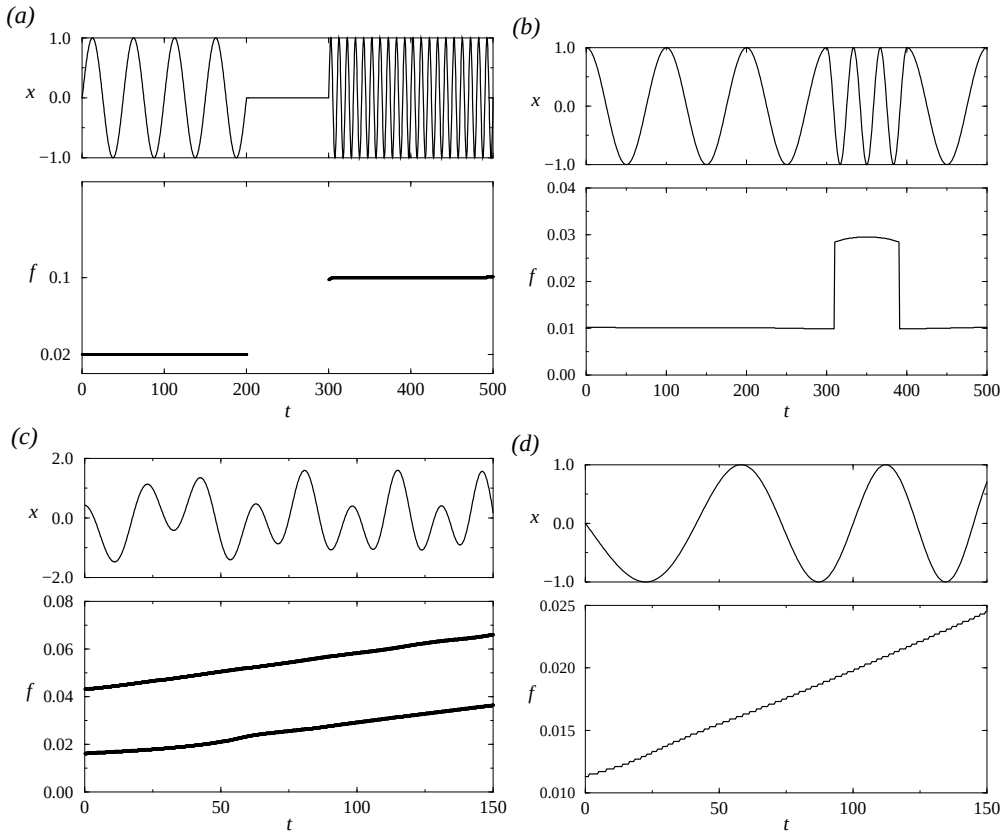

Figure 2.4: Top panels: Non-stationary time series. Bottom panels: frequency vs. time determined with wavelet transforms. (a) Two frequencies each appearing over different time intervals, (b)frequency switching between 0.01 and 0.03 Hz, (c) two superimposed signals, each with increasing frequency typical for TGF and the myogenic mechanisms, (d) Frequency increasing from 0.01 Hz, the lowest frequency observed in SHR recordings, to the doubled frequency within a single cycle.

shows a non-stationary time series used in Ref. (Chon et al., 2005) to illustrate the ability of a time frequency spectral method to extract different frequencies. The bottom panel shows the frequencies calculated with our wavelet method. The result is exactly the same as reported in Ref. (Chon et al., 2005). During the first 200 sec we detect a frequency of 0.02 Hz. During the following 100 sec no detection is made as the amplitude of the signal vanishes, and for the last 200 sec we detect a signal of 0.1 Hz. The top panel of Fig. 2.4b shows a time series in which the frequency of oscillation is switched from 0.01 Hz to 0.03 Hz. The bottom panel of Fig. 2.4b shows the result obtained with wavelet transforms. The change in frequencies is detected and over a time interval less than one cycle of the higher frequency. The top panel of Fig. 2.4c shows a time series resulting from the addition of two signals with linearly increasing frequencies. The result, shown in the bottom panel, is the same as reported in Ref. (Wang et al., 2006), although they extended the time series to higher frequencies. The top panel of Fig. 2.4d shows a time series that begins at the lowest TGF frequency we observed in SHR and that increases linearly with time to double within a single period of the initial cycle. The result obtained with wavelet transforms shows that the method accurately detects the frequency change. These results shows that wavelet methods provide frequency resolution comparable to time frequency spectral methods, a comparison that is well supported in the literature, and that they satisfy the frequency requirements of the data sets to which we have applied them.

2.1.2 Double-wavelet technique

To learn about the modulation process we need to estimate the frequency and depth of modulation. To study the modulation features of a fast oscillatory mode by a slower variable we propose to use the instantaneous frequencies $f_{fast}(t)$ and amplitudes $a_{fast}(t)$ of the fast rhythm, extracted via wavelet analysis, as input signals for a second wavelet transformation (2.1) as described in Ref. (Sosnovtseva et al., 2004). The obtained wavelet spectra will contain information about all components involved in the modulation process. In the case

of nonstationary dynamics we can examine how the features (characteristics) of modulation are changed in time.

Let us focus on the depth of modulation. For amplitude modulation, $M = \Delta A/A$ with $\Delta A = (A_{max} - A_{min})/2$ and A is the mean value. For frequency modulation, $M = \Delta\omega/\Omega$, where $\Delta\omega = (\omega_{max} - \omega_{min})/2$ and Ω is the modulation frequency. For nonstationary processes, $A(t)$ and $\Omega(t)$ are determined via a single wavelet while $\Delta A(t)$ and $\Delta\omega(t)$ are determined via the double-wavelet technique.

Possibilities and limitations of the double-wavelet method can be illustrated in different examples. For this purpose we consider the classical expressions for an amplitude, and a frequency modulated signal, expressed, respectively, by means of the two harmonic functions:

$$x(t) = A(1 + m \cdot \sin(\Omega t + \varphi)) \cdot \sin(\omega t + \varphi_0), \tag{2.4}$$

and

$$x(t) = A \sin\left[\omega t + m \cdot \sin(\Omega t + \varphi)) + \varphi_0)\right]. \tag{2.5}$$

We will take $A \in [1; 10]$, $m \in [0; 1]$, and $\omega = 2\pi \cdot 0.15$. Ω changes from $2\pi \cdot 0.03$ to $2\pi \cdot 0.02$. The phase variables φ and φ_0 assume random, but constant values.

Using the double-wavelet technique on time series generated by 2.4 and 2.5, it is possible to clearly distinguish two modes, associated with the frequencies Ω and ω, to extract the instantaneous amplitude (Fig. 2.5a) and the frequency (Fig. 2.6a) of the fast (modulated) mode and, by considering these variables as new signals, to estimate the modulation characteristics.

When performing such an analysis, a number of features of the method are revealed:

(i) Wavelets have some averaging effects that occur because the properties of a signal at the fixed time moment are studied within some a "window" defined by the function ψ. While the frequency of modulation is correctly estimated, the modulation depth M obtained from the wavelet analysis is approximately half

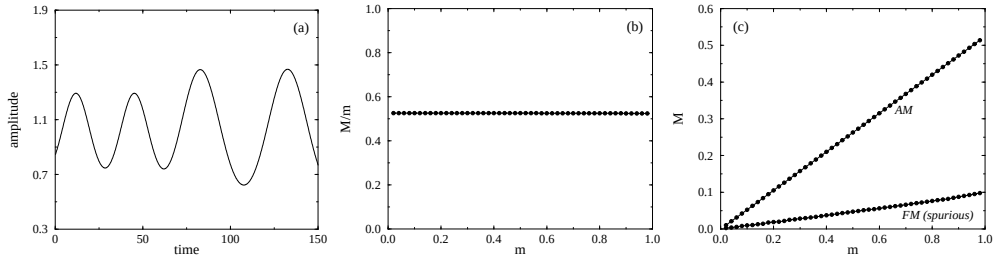

Figure 2.5: Analysis of amplitude modulation (AM) using the signal (2.4). (a) The instantaneous amplitude of the fast oscillatory mode extracted by means of wavelets; (b) The ratio M/m versus the parameter m; (c) The dependence of M versus m demonstrates the spurious effect of the frequency modulation (FM). Here, $A = 1$.

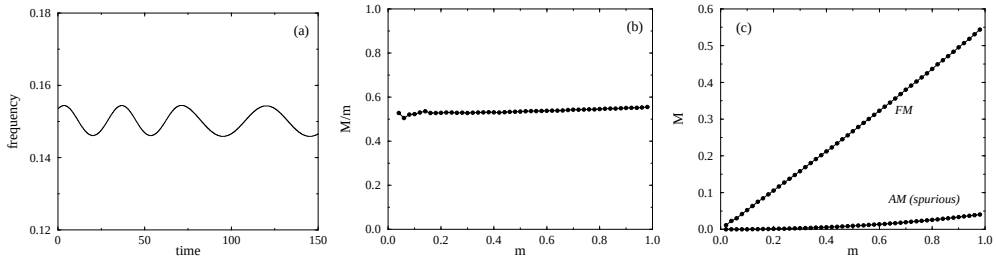

Figure 2.6: Analysis of frequency modulation using the signal (2.5). (a) The instantaneous frequency of the fast oscillatory mode extracted by means of wavelets; (b) The ratio M/m versus the parameter m; (c) The dependence of M versus m shows the spurious effect of the amplitude modulation.

of its true value m since we estimate averaged characteristics in a finite sized "window". However, for the amplitude modulation (Fig. 2.5b) the ratio M/m does not depend on the values of m and A, and there is only a weak dependence on m for the case of frequency modulation (Fig. 2.6b). Moreover, the values M/m practically coincide in Figs. 2.5b and 2.6b, i.e. the frequency and the amplitude modulations lead to the same averaging effect. The latter means that it is possible to correctly estimate the modulation depths by multiplying the results of the double-wavelet approach by a constant factor about 2.0 that we use in the subsequent analysis. (This factor can show some variations depending on the frequency of modulation and can be corrected if the frequencies ratio Ω/ω deviates significantly from the values considered in our examples).

(ii) In the case of pure amplitude modulation (Eq. (2.4)), the method can show spurious effects of a weak frequency modulation. This spurious modulation is approximately 5 times less in relative value than the actual amplitude modulation (Fig. 2.5c). By analogy, there may be spurious amplitude variations in the case of only frequency modulation, the latter effect being about 10 times less than the true modulation (Fig. 2.6c). In other words, if we deal with pure frequency or amplitude modulation we can expect to see additionally (weak) spurious modulations. Therefore, if both types of modulation are revealed in a data analysis, we must check whether their depths are comparable with the possible spurious effects.

(iii) The results of the double-wavelet approach are fairly insensitive to additive noise (fluctuations). We have added different types of noise to $x(t)$ (a $1/f$-like process modeling a slow nonstationarity and a normally distributed random process with intensities $[10^{-4}; 10^{-2}]$) and have observed that the obtained quantities for all practical purposes coincide with those presented in Figs. 2.5b,c and 2.6b,c.

To demonstrate the applications of our approach to the case of more complex dynamics we have considered the model of an electronic oscillator described by the following mathematical model (Anishchenko, 1995):

$$\dot{x} = kx + y - xz - bx^3,$$

$$\begin{aligned} \dot{y} &= -x, \\ \dot{z} &= -gz + gx(x + \mid x \mid)/2. \end{aligned} \tag{2.6}$$

Choosing different values for the control parameters k, g and b, it is possible to obtain a variety of dynamical regimes, including periodic and chaotic dynamics. In particular, the system (2.6) can produce a regime of self-modulated oscillations. This autonomous regime is characterized by slow oscillations for the variable z and fast oscillations for variables x and y (Sosnovtseva et al., 2002b). To illustrate the double-wavelet technique for nonstationary data, we have chosen the case of self-modulated oscillations in a regime of transient chaos. The dynamics of the fast variable of the model (2.6) suggests modulation by the slow rhythm (Fig. 2.7). The amplitude and the frequency of the fast oscillatory mode are changed in time with the period of slow dynamics.

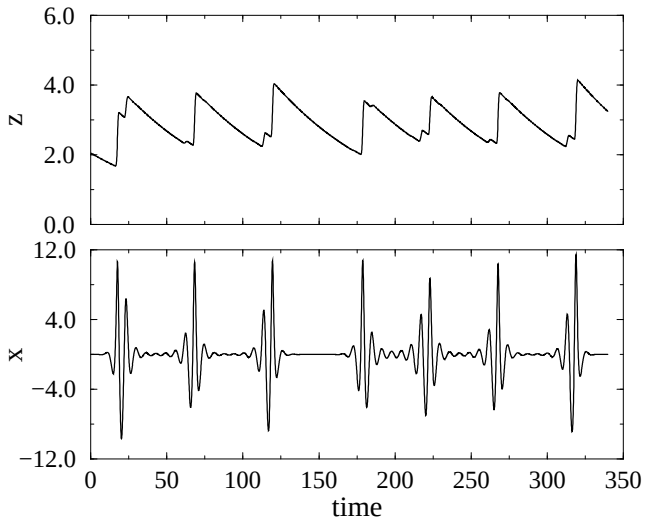

Figure 2.7: Time plots for the slow (z) and fast (x) variables in the model (5). Here, $k = 2.90328$, $g = 0.012505$, and $b = 5 \cdot 10^{-5}$.

For the considered regime, the instantaneous frequency of the fast mode extracted from the slow variable z, is shown in Fig. 2.8a. For part of the oscillatory period the frequency of the fast mode here takes values that are close to prominent harmonics of the slow rhythm, and the wavelet analysis can fail to distinguish between them. However, even missing some points, we are able to

estimate the frequency of modulation and the modulation depth by performing the wavelet transform for the extracted temporal dependence (Fig. 2.8a). Here, the depth of frequency modulation M_f takes the value ≈ 1.1 reflecting a strong frequency modulation (or self-modulation). Analysis of the instantaneous amplitude with the double-wavelet approach gives the value for the depth of amplitude modulation $M_a \approx 0.95$, i.e., we also deal with the case of strong amplitude modulation. The frequencies of modulation practically coincide with the instantaneous frequency of the slow mode (Fig. 2.8c), and the obtained values of the modulation depth correspond to the expected values, which can be approximately estimated from the time series of the fast variable x depicted in Fig. 2.7. Hence, we can state that the approach allows us to correctly estimate the properties of modulation in the case of complex multimode dynamics. Besides, we can be sure that the presence of a slow nonstationarity in the data (1/f-like processes) does not have an essential influence on the estimated characteristics.

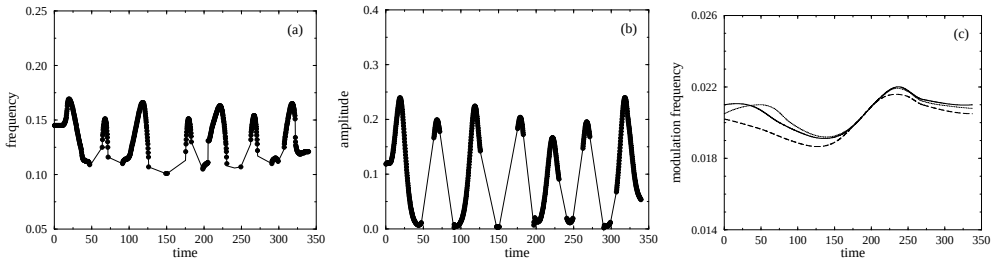

Figure 2.8: Instantaneous frequency (a) and amplitude (b) of the fast mode as extracted from the time series of the slow variable (z) of the model (5) for the case of self-modulated oscillations in the regime of transient chaos. Missing points can be interpolated. This approach is not crucial to correctly estimate the modulation properties, however. (c) The instantaneous modulation frequencies for amplitude (dashed) and frequency (dotted) modulation. Solid curve represents the instantaneous frequency of the slow dynamics.

Hence, we can follow the time evolution of characteristics such as the depth and frequency of modulation. In other words, the approach, that we will refer to as *double-wavelet analysis*, allows us to quantify the nonstationary temporal dynamics of a modulated signal, i.e., to detect all modes involved in the mod-

ulation, estimate the depth of modulation for each mode, and determine how the modulation properties change during the experimental observation period.

2.1.3 Frequency and phase entrainment

The order of synchronization is equal to n:m if m periods of external forcing correspond to n periods of response oscillations. Van der Pol seems to be the first who has investigated the response of the circuit to periodic forcing in a wide range of its frequencies (van der Pol, 1927). 1:m and m:1 synchronization was studied analytically by Hayashi (Hayashi, 1964) and Landa (Landa, 1980).

m:n phase synchronization between two oscillators is said to occur if

$$\mid n\Phi_2(t) - m\Phi_1(t) - C \mid < \mu, \tag{2.7}$$

where μ is a small parameter ($\mu < 2\pi$) that controls the allowed play in the phase locking. In particular, 1:1 phase synchronization is realized if the phase difference $\Phi_2(t) - \Phi_1(t)$ remains bound to a small interval μ around a mean value C.

For systems subjected to external disturbances or noise one can only expect the condition for phase synchronization to be satisfied over finite periods of time, interrupted by characteristic jumps in $\Delta\Phi$. Under these circumstances one can speak about a certain degree of phase synchronization if the periods of phase locking become significant compared to the characteristic periods of the interacting oscillators (Stratonovich, 1963). Alternatively, one can use the concept of frequency synchronization if the weaker condition

$$\Delta\Omega = \left\langle n\ \dot{\Phi}_2\ (t) - m\ \dot{\Phi}_1\ (t) \right\rangle = 0 \tag{2.8}$$

is satisfied. Here, $\langle\rangle$ denotes time average, and $\Delta\Omega$ is the difference in (mean) angular frequencies.

In contrast to periodic oscillations, chaos does not have a unique period, which makes introduction of a phase for chaotic oscillations quite a non-trivial problem. At the moment there is no unique way to introduce a phase for deter-

ministic chaos. However, quite often chaotic oscillations $x(t)$ can be considered as a narrow-band (quasi-)random process, for which it is known that it might be approximated by a signal with modulated phase and amplitude (Kuznetsov et al., 1965)

$$x(t) = A(t)\cos\Phi(t) = A(t)\cos\left(\omega_0 t + \varphi(t)\right), \tag{2.9}$$

where $A(t) \geq 0$ is a random amplitude and $\varphi(t)$ is a random phase. In spite of its simplicity, such approximation has been shown quite accurate to describe the statistical properties of a wide class of chaotic oscillations, e.g. of those born as a result of a cascade of period-doubling bifurcations.

One of the most popular ways to define the amplitude $A(t)$ and the phase $\Phi(t)$ in Eq. (2.9) involves Hilbert transform (Gabor, 1946; Kuznetsov et al., 1965). Two signals $x(t)$ and $y(t)$ are connected via Hilbert transform, if

$$x(t) = -\frac{1}{\pi}\int_{-\infty}^{\infty}\frac{y(t')}{t-t'}dt', \qquad y(t) = \frac{1}{\pi}\int_{-\infty}^{\infty}\frac{x(t')}{t-t'}dt', \tag{2.10}$$

where the integrals are taken in the sense of Cauchy principal values. Then we can formally introduce a complex signal $\eta(t)$ often called analytic signal as follows

$$\eta(t) = A(t)\exp\left(i\Phi(t)\right) = A(t)\exp\left[i(\omega^0 t + \varphi(t))\right] = x(t) + iy(t). \tag{2.11}$$

We require that $y(t)$ is expressed as

$$y(t) = A(t)\sin\Phi(t) = A(t)\sin\left(\omega^0 t + \varphi(t)\right), \;\; |A(t)| \geq 0, \;\; |\varphi| \leq \pi, \tag{2.12}$$

and is a Hilbert transform of $x(t)$, which is the real part of analytic signal $\eta(t)$. Using the functions $x(t)$ and $y(t)$, the instantaneous amplitude $A(t)$ and the instantaneous phase $\Phi(t)$ can be defined unambiguously as

$$A(t) = |\eta(t)| = \sqrt{x^2(t) + y^2(t)}, \tag{2.13}$$

$$\Phi(t) = \arg(\eta(t)) = \tan^{-1}(y(t)/x(t)). \tag{2.14}$$

In this case the phase Φ can be geometrically understood as an angle of rotation

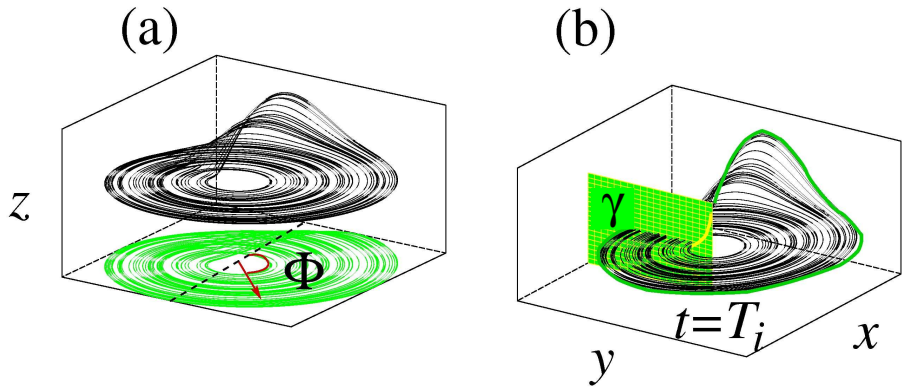

Figure 2.9: Two ways to introduce phase for chaotic oscillations: (a) as an angle of rotation of the phase trajectory in some projection; (b) via times T_i of trajectory return to a certain Poincaré secant surface γ.

of a vector with the amplitude $A(t)$ in some projection plane (x, y) as shown in Fig. 2.9a.

If one presumes that the 2π growth of phase corresponds to one full rotation of the phase trajectory around some center, Poincaré section technique can sometimes be used for the introduction of the phase. As illustrated in Fig. 2.9b, one can define a Poincaré secant surface γ and collect time moments T_i at which the phase trajectory crosses the surface γ in the chosen direction, e.g. from left to right. Between two successive intersections, i.e. during the time interval $(T_{i+1} - T_i)$ the phase grows linearly by 2π. Then we can express phase Φ at any time moment t as

$$\Phi(t) = \frac{t - T_i}{T_{i+1} - T_i} + 2\pi i. \tag{2.15}$$

Note that in order to be able to introduce phase like this, it is important to define the section γ to be transversal to *all* phase trajectories on the attractor and in its vicinity. Otherwise some rotations of the phase trajectory might not be taken into account, and the quantity Φ might have essentially non-monotonous character. In case when chaotic oscillations cannot be treated as a narrow-band signal, the correct introduction of the phase becomes quite a complicated problem.

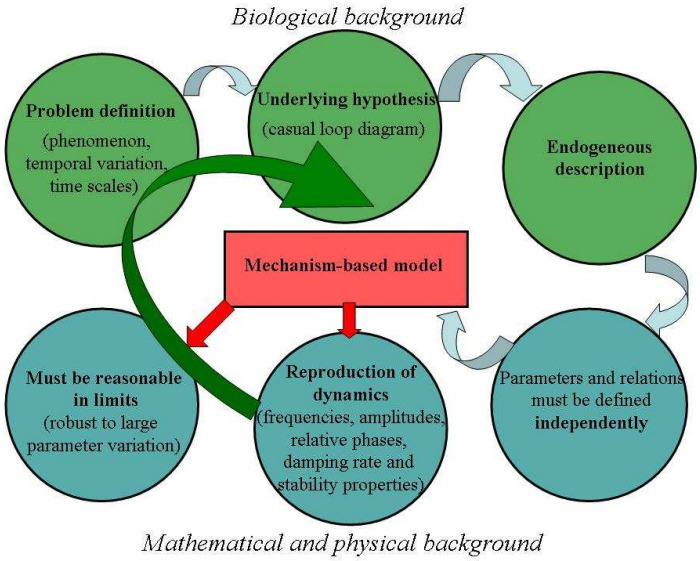

Figure 2.10: Illustration of the main aspects of mechanism-based modeling. Note in particular the important role of problem definition. It is through this process that one can separate different time scales and decide what is important and what is not.

2.2 Modeling approach

Mechanism-based modeling stems from engineering and other fields of science that have strong theoretical traditions. Computer simulation allows engineers to test the function of a new construction and compare it with other possible constructions long before the first prototype is made. The results are enormous savings in time and money. Direct application of the same approach to biomedical problems is primarily restricted by the overwhelming complexity of living systems. From physics we have inherited the idea that one can separate processes and phenomena based on their temporal and spatial scales. This is obviously much more difficult for biological systems with their many and strongly coupled processes at overlapping time and space scales. Moreover, some of the most interesting problems are precisely to explain the coordination of processes that occur over separate time scales or to explain the properties of a tissue or the function of an organ in terms of the processes and interactions of the constituting cells or functional units.

Hypothesis-driven, or mechanism-based modeling is an approach in which the physiological, pathological and pharmacological processes of relevance to a given problem are represented as directly as possible. This approach allows us (i) to test whether assumed hypotheses are consistent with observed behavior, (ii) to examine the sensitivity of a system to parameter variation, (iii) to learn about processes not directly amenable to experimentation.

In mechanism-based modelling the starting point is a dynamic hypothesis about the processes underlying a particular phenomenon. The modelling is not restricted by linearity assumptions, nor is it restricted by the possibility of estimating the parameters from a particular experiment. The idea is that the structure of the model should present the available knowledge about the linear and nonlinear interactions and about the positive or negative feedback regulations as completely and consistently as possible. All parameters and relations are assumed to be obtained from independent experiments. Such a model is validated through its ability to generate behaviours with amplitudes, periodicities, phase relationships, response dynamics, damping characteristics, and stability properties in accordance with the experimentally observed dynamics (Mosekilde et al., 2005). At the end, the model is validated by its ability to predict phenomena not previously experienced.

Chapter 3

Model

3.1 Single nephron model

Over the years significant efforts have been made to develop mathematical models that can account for the observed regular and irregular pressure variations and describe the physiological processes that occur along the tubular system (Jensen et al., 1986; Holstein-Rathlou and Leyssac, 1987; Holstein-Rathlou and Marsh, 1990; Barfred et al., 1996; Pitman et al., 2004; Thomas et al., 2006). A particular aspect of this research has been to show that the transition from regular oscillations to irregular variations in the tubular pressure can be explained in terms of parameter changes within the framework of well-established physiological mechanisms.

3.1.1 Pressure variations

The pressure P_t in the proximal tubule changes in response to differences between the in- and outgoing fluid flows

$$\dot{P}_t = \left[F_{filt}(P_t, P_a, r) - F_{reab} - F_{Hen}\right]/C_{tub}. \tag{3.1}$$

Here the incoming flow, the glomerular filtration rate F_{filt}, is expressed as a function of the tubular pressure P_t, arterial pressure P_a and radius of the afferent arteriole r. Details are given in Ref. (Holstein-Rathlou and Leyssac, 1987) F_{reab}

is the rate of tubular fluid reabsorption in the proximal tubule, F_{Hen} is the flow of fluid into the loop of Henle, and C_{tub} is the elastic compliance of the tubule. The Henle flow is determined by the difference between the proximal (P_t) and the distal (P_d) tubular pressures and by the flow resistance R_{Hen}: $F_{Hen} = (P_t - P_d)/R_{Hen}$. In the present model, the reabsorption F_{reab} in the proximal tubule and the flow resistance R_{Hen} are treated as constants. This description is clearly a simplification. However, within the physiologically relevant flow range the expression provides a good approximation to the experimentally determined pressure-flow relation. Reabsorption processes are accounted for in considerable detail in the spatially extended model developed in Ref. (Holstein-Rathlou and Marsh 1990).

3.1.2 Tubuloglomerular feedback

Tubuloglomerular feedback (TGF) exerts its effects on the afferent arteriole, reducing its radius in response to increasing NaCl concentrations at the macula densa. In the usual experimental evaluation of the TGF mechanism in open-loop experiments (Leyssac and Holstein-Rathlou, 1989), the flow rate into the loop of Henle is the independent variable, glomerular filtration rate is clamped at 0, and one measures a change in proximal tubule pressure as a reflection of the resistance of the afferent arteriole . The effect of changes in the loop of Henle flow can be described by a sigmoidal relation between the muscular activation ψ of the afferent arteriole and the delayed Henle flow

$$\Psi = \Psi_{max} - \frac{\Psi_{max} - \Psi_{min}}{1 + exp(\alpha(3X_3/TF_{Hen0} - S))} \tag{3.2}$$

where Ψ_{max} and Ψ_{min} are the upper and lower activation limits of TGF mechanism, α is the maximum slope and S the inflection point of the S-shaped curve that characterizes the TGF relation. α is usually refered to as the TGF feedback gain. $3X_3/T$ is a delayed version of the flow into the loop of Henle and F_{Hen0} is a normalized value of the loop of Henle flow.

3.1.3 Afferent arteriole

The afferent arteriole is modeled as a damped second order system

$$\ddot{r} + d\dot{r} = \frac{P_{av} - P_{eq}}{\omega} \tag{3.3}$$

where, as before, r is the afferent arteriolar radius, normalized to its resting value, and P_{av} and P_{eq} are, respectively, average and equilibrium values of the vascular pressure in the arteriole. d is a dampling coefficient, and ω is a parameter that controls the dynamic characteristics of the myogenic oscillations. The subscript av on the pressure P_{av} refers to the fact that this pressure is evaluated as the average hydrostatic pressure along the length of the afferent arteriole:

$$P_{av} = \frac{1}{2}(P_a - (P_a - P_g)\beta\frac{R_{a0}}{R_a} + P_g) \tag{3.4}$$

with the glomerular pressure given by

$$P_g = P_v + R_e(\frac{P_a - P_g}{R_a} - F_{filt}) \tag{3.5}$$

Equations (3.4) and (3.5) express simple linear relations between flow rates and pressure drops in the arteriolar system. P_v is the venous pressure, and R_a and R_e are the flow resistances of the afferent and the efferent arterioles. β is the fraction of the total afferent arteriolar length that responds to the TGF signal, and R_{a0} is a resting value of R_a.

$$P_{eq} = 0.006exp(10(r-0.8)) + 1.6(r-1) + \Psi(\frac{4.7}{1+exp(13(0.4-r))} + 7.2(r+0.9)) \tag{3.6}$$

is the hydrostatic pressure at which the afferent arteriole is at equilibrium for a given muscular activation Ψ and a given radius r. Terms that are independent of Ψ represent the nonlinear elastic deformation of the vascular wall, and terms proportional to Ψ represents the active (myogenic) response. Equation (3.6) was obtained through a combination of theoretical considerations and curve

fitting to experimental results.

3.1.4 Delay

Regulation of pressures and flows in the nephron is dominated by the negative feedback associated with the TGF mechanism. However, there is a delay in this feedback associated with the time it takes for a flow change to propagate from the glomerulus through the loop of Henle and from the cascaded enzymatic processes between the macula densa cells and the smooth muscle cells of the afferent arteriole. The model represents this delay as a 3rd order delay structure:

$$\dot{X}_1 = F_{Hen} - \frac{3}{T}X_1 \tag{3.7}$$

$$\dot{X}_2 = \frac{3}{T}(X_1 - X_2) \tag{3.8}$$

$$\dot{X}_3 = \frac{3}{T}(X_2 - X_3) \tag{3.9}$$

where T is the total delay time, and $3X_3/T$ is the delayed flow that serves as an input to the TGF mechanism (3.2).

The feedback delay, which typically assumes a value of 12-18 *sec*, will be considered a bifurcation parameter in our analysis. Another important parameter is the strength α of the feedback regulation. This parameter takes a value of about 12 for normotensive rats, increasing to about 18 for hypertensive rats (Leyssac and Holstein-Rathlou, 1989).

The single nephron model (Barfred et al., 1996) consists of a set of five coupled differential equations expressing the rate of change of the proximal tubular pressure, the oscillatory dynamics of the afferent arteriolar radius, and the delay associated with the flow of fluid through the loop of Henle. The main nonlinearities of the model are related to the feedback regulation of the arteriolar radius and to the relation between this radius, the degree of activation of the arteriolar smooth muscles, and the equilibrium pressure in the arteriole. Other nonlinearities are associated with the relation between the radius and the flow resistance of the arteriole and between the tubular pressure and the

glomerular filtration rate.

3.2 Coupled nephron model

Neighboring nephrons can influence each other's blood supply either through vascularly propagated electrical (or electrochemical) signals or through a hemodynamic coupling arising via a direct redistribution of the blood flow between the coupled nephrons. While the hemodynamic coupling depends mainly on the flow resistances in the arteriolar network, the vascularly propagated coupling is associated with signal transmission between smooth muscle cells. The result is that only nephrons situated close to one another can interact via the vascularly propagated coupling. Nephrons situated farther apart but sharing a common piece of interlobular artery may interact via the hemodynamic coupling.

3.2.1 Vascularly propagated coupling

In the present work we shall focus our attention on the vascularly propagated coupling, assuming the hemodynamic coupling to be negligible. In the single-nephron model the equilibrium pressure in the afferent arteriole depends on the current radius r and on the activation level Ψ of the smooth muscles surrounding the arteriole and controlling its diameter. The muscular activation arises at the juxtaglomerular apparatus and travels upstream along the afferent arteriole in a damped fashion. When it reaches the branching point with the arteriole from the neighboring nephron, part of the signal may propagate down that arteriole and start to contribute to its TGF response. The coupling is considered nearly instantaneous since the time it takes for the vascular signal to reach the other nephron is very small relative to the period of the TGF-oscillations. It has been observed that the signal decreases nearly exponentially as it propagates (Chen et al., 1995). Thus only a fraction, $\gamma = e^{-l/l_0} < 1$, of the original activation level reaches the vascular smooth muscles close to macula densa of the neighboring nephron. In the expression for the vascular coupling parameter γ, l is the propagation length of the coupling signal, and $l_0 \cong 500\ \mu m$ is the characteristic

length scale of the exponential decay. In the model, the vascularly propagated coupling is represented by adding a contribution of the activation level in one nephron to the activation level in the neighboring nephron:

$$\Psi^*_{1,2} = \Psi_{1,2} + \gamma\Psi_{2,1} \tag{3.10}$$

with γ being the coupling parameter and $\Psi_{1,2}$ the uncoupled activation levels of the two nephrons as determined by their respective Henle flows. In view of the characteristic propagation length for the signal and of measured distances between neighboring nephrons along the arteriolar network, a typical value of γ is considered to be 0.1 - 0.2 (Chen et al., 1995).

3.2.2 Hemodynamic coupling

To implement the hemodynamic coupling, a piece of common interlobular artery is included in the system, and the total length of the incoming blood vessel is hereafter divided into a fraction $\varepsilon < \beta$ that is common to the two interacting nephrons, a fraction $1 - \beta$ that is affected by the TGF signal, and a remaining fraction $\beta - \varepsilon$ for which the flow resistance is considered to remain constant. As compared with the equilibrium resistance of the separate arterioles, the piece of shared artery is assumed to have half the flow resistance per unit length.

Defining P_ε as the pressure at the branching point of the two arterioles, the equation of continuity for the blood flow reads

$$\frac{P_a - P_\varepsilon}{\varepsilon R_{a0}/2} = \frac{P_\varepsilon - P_{g1}}{R_{a1}} + \frac{P_\varepsilon - P_{g2}}{R_{a2}} \tag{3.11}$$

with

$$R_{a1} = (\beta - \varepsilon)\, R_{a0} + (1 - \beta)\, R_{a0} r_1^{-4} \tag{3.12}$$

and

$$R_{a2} = (\beta - \varepsilon)\, R_{a0} + (1 - \beta)\, R_{a0} r_2^{-4}. \tag{3.13}$$

Here, R_{a0} denotes the total flow resistance for each of the two arterioles in equilibrium. r_1 and r_2 are the normalized radii of the active part of the afferent arterioles for nephron 1 and nephron 2, respectively, and P_{g1} and P_{g2} are the corresponding glomerular pressures. As a base value of the hemodynamic coupling parameter we shall use $\varepsilon = 0.2$.

Because of the implicit manner in which the glomerular pressure is related to the efferent colloid osmotic pressure and the filtration rate, direct solution of the set of seven coupled algebraic equations for the two-nephron system becomes rather inefficient. Hence, for each nephron we have introduced the glomerular pressure P_g as a new state variable determined by

$$\frac{dP_{g,i}}{dt} = \frac{1}{C_{glo}} \left(\frac{P_\varepsilon - P_{g,i}}{R_{a,i}} - \frac{P_{g,i} - P_v}{R_e} - F_{filt,i} \right) \tag{3.14}$$

with $i = 1, 2$. This implies that the glomerulus is considered as an elastic structure with a compliance C_{glo} and with a pressure variation determined by the imbalance between the incoming blood flow, the outgoing blood flow, and the glomerular filtration rate. From a physiological point of view, this formulation is well justified. Compared with the compliance of the proximal tubule, C_{glo} is likely to be quite small, so that the model becomes numerically stiff. In the limit $C_{glo} \to 0$, the set of differential equations reduces to the formulation with algebraic equations presented in single nephron model. Finite values of C_{glo} will change the damping of the system, and therefore also the details of the bifurcation structure. In practice, however, the model will not be affected significantly as long as the time constant $C_{glo}R_{eff}$ is small compared with the periods of interest. Here, $1/R_{eff} = 1/R_a + R_e$.

3.3 Vascular model

Our model includes both vascular and nephron components. The interactions among the nephrons occur via vascular signal propagation and due to oscillations in vascular pressure within the cortical radial artery. We make use of a relatively simple model of nephron dynamics (Holstein-Rathlou and Leyssac

1987; Barfred et al., 1996) and consider a tapering cortical radial artery whose dimensions are based on recent measurements made in rat kidneys (Nordsletten et al., 2006).

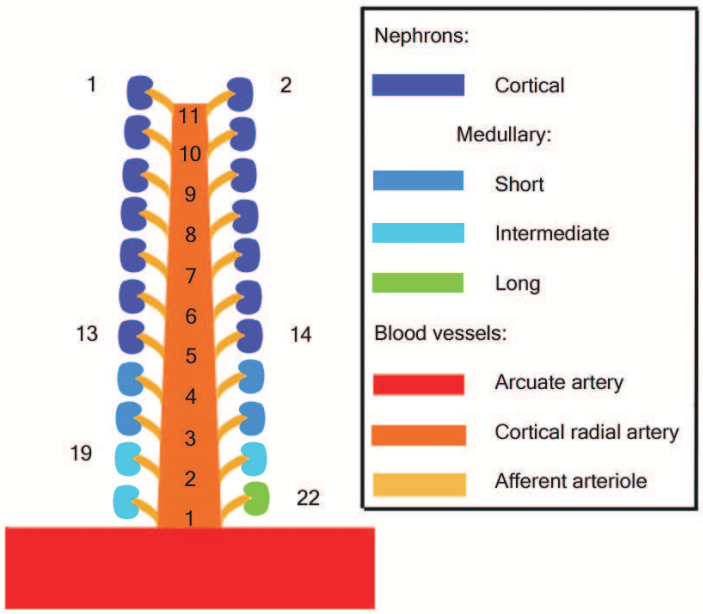

Figure 3.1: Structure of the vascular tree that was modeled; nephrons are depicted by showing their glomeruli. Blood flows from the arcuate artery into the cortical radial artery. Twenty two nephrons receive blood through afferent arterioles from the cortical radial artery. Nephrons are numbered laterally, and the vascular nodes of origin of the afferent arterioles are numbered within the cortical radial artery.

We used 22, of which 14 were defined as cortical and 8 as medullary. Figure 3.1 shows the anatomic basis for the vascular model. A tapered cortical radial artery branches from an arcuate artery. One pair of afferent arterioles branches from the arcuate artery and ten pairs from the cortical radial artery. The level of origin of each pair is designated a node. At the 9th node, for example, conservation of blood flow yields:

$$\frac{P_8^b - P_9^b}{R_8^b} - \frac{P_9^b - P_{10}^b}{R_9^b} - \frac{P_9^b - P_5^g}{R_5^g} - \frac{P_9^b - P_6^g}{R_6^g} = 0 \tag{3.15}$$

where the superscript b refers to the branching arteriole, and the superscript g to the glomerulus. The values of R_k^b are calculated as $8\eta l_k/\pi r_k^4$, using a blood viscosity η of 4.6 $cPoise$ (1 $cPoise = 10^{-3}\ kg/m \cdot s$), a segment length of 0.02 cm, and radius values r_k taken from the literature (Nordsletten et al., 2006). Values of P^g and R^g are calculated in the nephron model with P_a corresponding to P_k^b and R_a corresponding to R_a^b. This formulation (3.15) is based on the assumption that the vascular tree can be described as purely resistive and that short term, local accumulation of blood can be neglected.

The contribution to the activation of the smooth muscle cells in the arterial wall of the jth nephron produced from vascularly propagated signals from the neighboring nephrons, $\Delta\Psi_j$, is modeled by:

$$\Delta\Psi_j = \sum_{i=1, i\neq j}^{N} \theta\Psi_i exp(-\lambda(L_{ji} + 2L^g)) \tag{3.16}$$

where Ψ_i is the TGF activation potential of TGF for the ith nephron as calculated from the nephron model. L_{ji} is the distance from the origin of jth to the origin of the ith afferent arteriole along the cortical radial artery; L^g is the length of the afferent arteriole, assumed identical for all nephrons; and λ is a length constant characterizing the exponential decrease of the vascular propagated signal along the blood vessels. θ is a control parameter that we use to examine the effects of different coupling strengths. $\theta = 0.25 - 0.50$ is considered the range of physiologically realistic values for animals with normal blood pressure. Twice the value of L^g is used because the TGF signal must be propagated down the afferent arteriole of the TGF mechanism that initiates the signal, and up the afferent arteriole of the TGF mechanism receiving it. Equation (3.16) expresses the current state of knowledge of the interaction: a change in the TGF signal in one nephron can be detected in the TGF mechanism of a neighboring nephron, and the effect of the interaction decreases exponentially with the vascular distance the signal must traverse (Källskog and Marsh, 1990; Chen et al., 1995; Wagner et al., 1997). The mechanisms underlying these interactions are presently not known in detail.

A number of studies report measurements of oscillations of tubular pressure

from cortical nephrons on the surface of the rat kidney. The period length of the TGF oscillation is $30-50$ s. The nephron model used in this study requires a value for the time delay of 12 s to reproduce a 30 s period, and this value was used as the starting point for all calculations with cortical nephrons. There are no measurements of proximal tubule pressure in juxtamedullary nephrons. A more detailed model (Marsh et al., 2005) was used to estimate the effect of increasing tubular length on the oscillation period. The inner medulla in the rat is 0.5 cm long. Adding descending and thin ascending limbs to this length increases the period about 50%. Different nephrons penetrate to intermediate depths of the inner medulla. The increase in period is likely to vary in proportion to the length of the segment. The inner medulla is conical in the rat, and the density of medullary nephrons is approximately constant over the volume of the inner medulla. This suggests that the number of nephrons decrease with increasing depth. In addition to the 14 cortical nephrons, we have therefore used 4 medullary nephrons that turn at a depth of $0.1cm$ in the inner medulla, 3 nephrons that reach $0.3cm$, and 1 nephron that reaches a depth of $0.5cm$. The assumed time delays were 14.0 s, 16.3 s, and 17.6 s, respectively, and 12.0 s for the cortical nephrons.

An important issue we wish to address in this paper is to what extent synchronization occurs among nephrons in the ensemble. If all the cortical nephrons have a single value of the time delay, and all the short medullary nephrons another single value, and so on, the question may be relatively simple. We have therefore introduced variation in the time delays by adding random numbers to the time delay in each of the 22 nephrons. The distribution of random numbers was Gaussian with a zero mean and a standard deviation of 0.4 s. A fixed value of the delay was used in each nephron for each run.

The nephron models were solved with a fourth order Adams Moulton predictor - corrector method using a fixed time step of $1 \times 10^{-4}s$. All nephron models were solved at each time step, and the pressure at each of the nodes in the cortical radial artery was calculated.

Chapter 4

Results

4.1 Multimodal dynamics in autoregulation

4.1.1 Rhythmic componenets

Individual nephron

While for normal rats the oscillations have the appearance of a limit cycle with a sharply peaked power spectrum, highly irregular oscillations, displaying a broadband spectral distribution with significant subharmonic components, are observed for spontaneously hypertensive rats (Holstein-Rathlou and Leyssac, 1986).

Figure 4.2 shows the different components detected in the time series of Fig. 4.1. Inspection of the figure reveals that the slow oscillations, whether they are periodic or chaotic, maintain a nearly constant frequency through the observation time. The fast oscillations, on the other hand, fluctuate around some average value. This may be related to a complex modulation of the fast oscillations by the slow dynamics or to the influence of noise (since the fast oscillations are small in amplitude, they are more sensitive to fluctuations). However, this picture does not give information about the dominant spectral components. This information can be obtained, for example, from a *scalogram*, i.e., a time averaged power spectrum, being an analogue to the Fourier power spectrum. Such a scalogram is illustrated in Fig. 4.3 where a well-pronounced

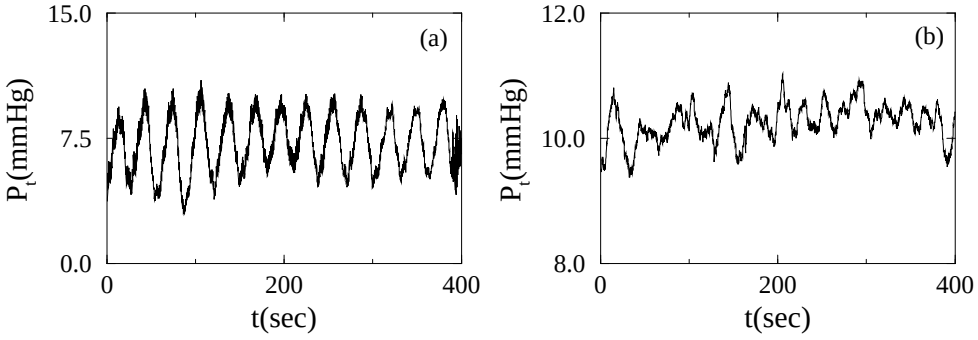

Figure 4.1: Regular tubular pressure oscillations from a normotensive rat (a) and irregular pressure variations from a spontaneously hypertensive rat (b).

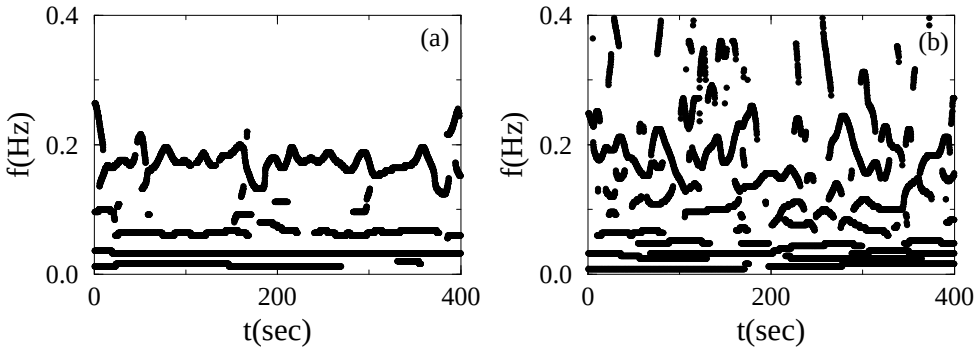

Figure 4.2: Wavelet analysis of the two time-series presented in Fig. 4.1.

peak around 0.03Hz, corresponding to the slow TGF-mediated mode, is distinguishable. The other peak at $0.15 - 0.2$Hz derives from the fast myogenic dynamics. It is interesting to note how clearly these oscillations can be detected from the tubular pressure variations. Since both the above frequency components are of physiological interest we extract them from the original wavelet transformation for further analysis of their coherence properties. Figure 4.4 displays the relation between fast and slow oscillations in a single nephron. For the periodic oscillations observed for normotensive rats (Fig. 4.4a), the fast and slow components adjust their periods in accordance to one another to maintain a $1 : 4$ entrainment during the observation time. For the chaotic oscillations observed for hypertensive rats (Fig. 4.4b), the ratio changes more randomly in time.

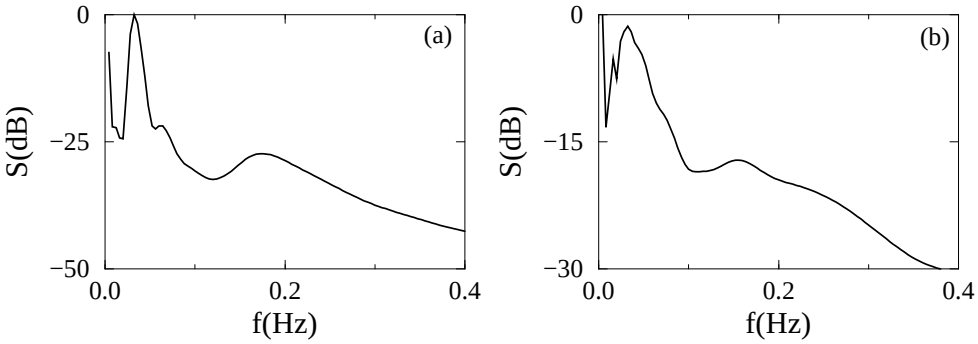

Figure 4.3: Power spectrum obtained from the wavelet analysis for the two time-series presented in Fig. 4.1. Two peaks, representing the fast myogenic oscillations and the slower tubuloglomerular oscillations, are well-distinguished.

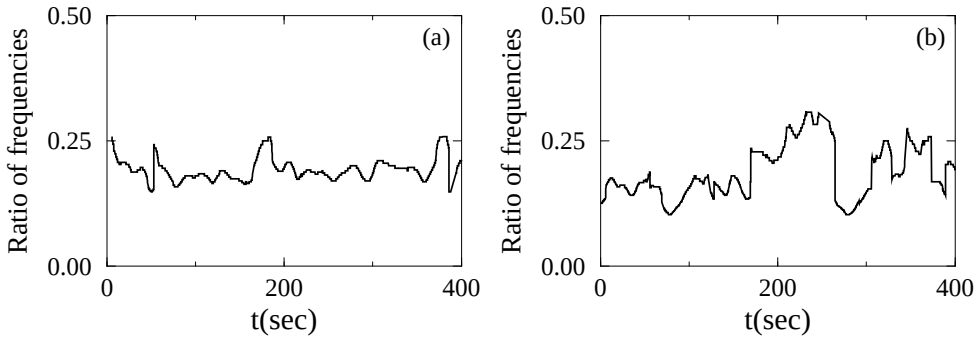

Figure 4.4: Ratio of the internal time-scales for a normotensive rat (a) and for a hypertensive rat (b). Note the $1:4$ synchronization for the normotensive rat.

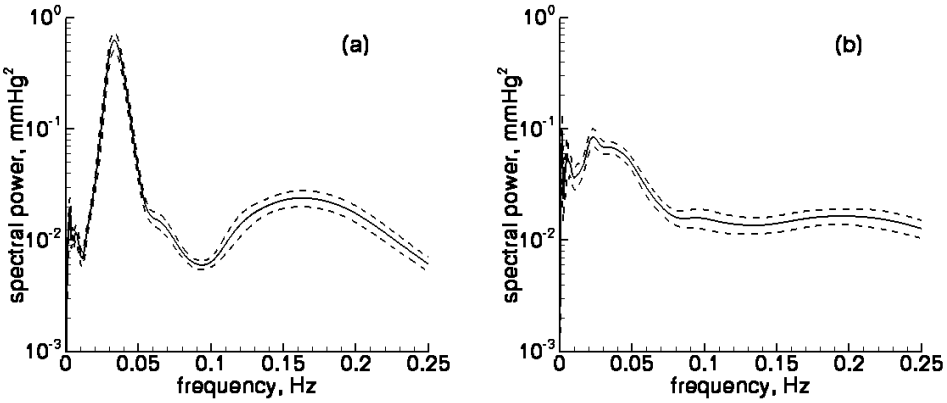

Figure 4.5: Averaged power spectra of tubular pressure variations for 32 time series from normotensive rats (a) and 42 time series from SHR (b). Values are shown as mean 1 SE.

Statistical analysis

Averaged power spectra for 32 time series from normotensive rats are in Fig. 4.5a and 42 time series from SHR in Fig. 4.5b. The analyzed time series for tubular pressure varied in length from 240 to 1260 sec, and were sampled at rates designed to produce time series of 4096 points. The spectrum from normotensive rats shows a sharp peak at a frequency of about 0.03 Hz corresponding to the slow TGF-mediated oscillations and a wider peak from the myogenic mechanism in the range $0.10 - 0.20$ Hz. The same peaks can be detected in the data from hypertensive rats although they are significantly smaller and broader, reflecting the irregularity of the signal. These results were obtained by calculating single power spectra from each experimental time series and averaging all the power spectra in each group of animals, a method that provides no temporal resolution.

Let us consider the case of intra-nephron interaction of the two modes. Figure 4.6 shows distributions of the ratio $f_{fast}(t)/f_{slow}(t)$, where $f_{slow}(t)$ and $f_{fast}(t)$ are the frequencies of the TGF-mediated and the myogenic oscillations, respectively. The distribution obtained for normotensive rats, shown in Fig. 4.6a, has 2 peaks corresponding to the ratios 4 and 5. This implies that the fast and the slow components adjust their periods in such a way as to maintain a near 4:1 or 5:1 entrainment during significant parts of the observation time.

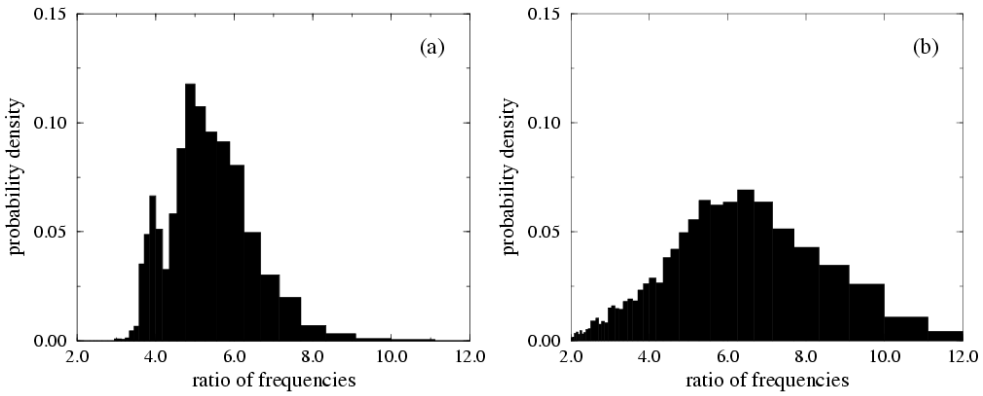

Figure 4.6: Distribution of the ratio of the instantaneous frequencies of myogenic and TGF-mediated oscillations from 32 time series in normotensive rats (a) and 42 time series in SHR (b).

The shoulder on the left hand side of the 5:1 indicates the presence of intervals with 6:1 synchronization. For the chaotic oscillations observed for the hypertensive rats, shown in Fig. 4.6b, the frequency ratio changes more randomly in time. There is only a single broad peak in the probability density, and the nephron dynamics show mutual adjustments only for time intervals that are too short to be clearly expressed in the averaged distribution of the ratio.

The self-sustained pressure fluctuations due to TGF can be periodic or chaotic in each nephron, and, so far as is known, the myogenic oscillations are periodic. The fluctuations from each mechanism can be synchronous or asynchronous with respect to each other in a single nephron.

Simulation

Both experimental investigations and simulations reveal one of the most important features of the single-nephron model, namely the presence of two different time scales in the pressure and flow variations. Considering the single nephron model one can identify the two time scales: (i) a low-frequency (TGF-mediated) oscillation with a period $T_h \cong 2.2T$ arising from the delay in the tubuloglomerular feedback, and (ii) somewhat faster oscillations with a period $T_v \approx T_h/5$ associated with the inherent myogenic adjustment.

To determine T_h and T_v, the mean return times of the trajectory to appro-

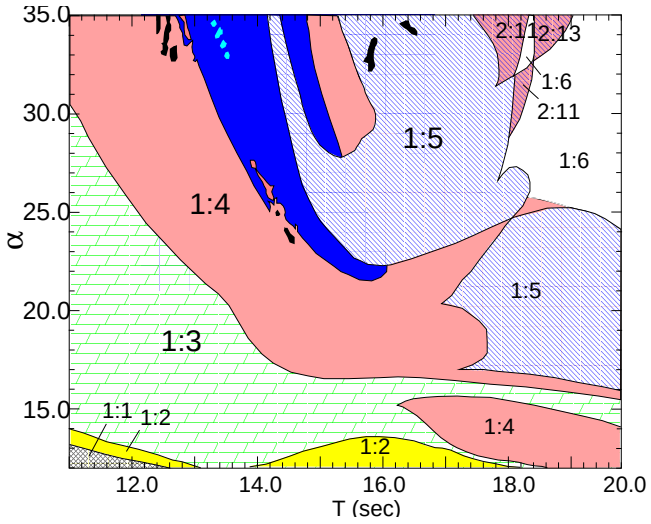

Figure 4.7: Two-mode oscillatory behavior in the single nephron model. Black colored regions correspond to a chaotic solution.

priately chosen Poincaré sections have been used:

$$T_v = < T_{ret} \mid_{\dot{v}_r=0} > \tag{4.1}$$

$$T_h = < T_{ret} \mid_{\dot{X}_2=0} > . \tag{4.2}$$

From these return times it is easy to calculate the intra-nephron rotation number (i.e., the rotation number associated with the two-mode behavior of the individual nephron)

$$r_{vh} = T_v/T_h. \tag{4.3}$$

This measure will be used to characterize the various forms of frequency locking between the two modes. With varying feedback delay T and varying slope α of the open loop feedback curve, Fig. 4.7 shows how the two oscillatory modes can adjust their dynamics and attain states with different rational relations $(n : m)$ between the periods. The regions of high resonances $(1 : 4,\ 1 : 5,$ and $1 : 6)$ are seen to exist in the physiologically interesting range of the delay time $T \in [12\ s, 20\ s]$.

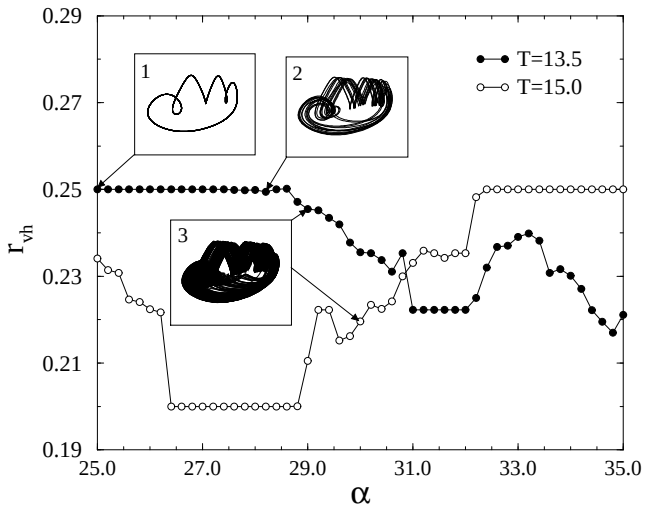

Figure 4.8: Internal rotation number as a function of the parameter α calculated from the single-nephron model. Inserts represent phase projections of typical regimes.

While the transitions between the different locking regimes always involve bifurcations, bifurcations may also occur within the individual regime. A period-doubling transition, for instance, does not necessarily change r_{vh}, and the intra-nephron rotation number may remain constant through a complete period-doubling cascade and into the chaotic regime. This is illustrated in Fig. 4.8 where we have plotted r_{vh} as a function of the feedback gain α for different time delays $T_2 = 13.5\ s$ (black circles) and $T = 15.0\ s$ (open circles). Phase projections (P_t, r) from the various regimes are shown as inserts. Inspection of the figure clearly shows that r_{vh} remains constant under the transition from regular $1:4$ oscillations (black circles for $\alpha = 25.0$) to chaos (for $\alpha = 28.0$), see inserts 1 and 2. With further evolution of the chaotic attractor (insert 3), the $1:4$ mode locking is destroyed. In the interval around $\alpha = 31.5$ we observe $2:9$ mode locking. A similar transition is observed for $T = 15\ s$ (open circles). Periodic $1:5$ oscillations ($\alpha = 27.0$) evolve into a chaotic attractor ($\alpha = 28.5$), but the rotation number maintains a constant value. For fully developed chaos, the $1:5$ locking again breaks down.

We conclude that besides being regular or chaotic, the self-sustained pres-

sure variations in the individual nephron can be classified as being synchronous or asynchronous with respect to the ratio between the two time scales that characterize the fast (arteriolar) mode and the slow (TGF mediated) mode, respectively. As we shall see, this complexity in behavior may play an essential role in the synchronization between a pair of interacting nephrons.

4.1.2 Frequency and amplitude modulation

Individual recording analysis

Despite the emergence of a consensus on the combined participation of both the myogenic and the TGF mechanisms in autoregulation, there are only a few attempts to examine the interplay between them. Let us consider recordings of tubular pressure from a single nephron in order to compare experimental and simulation results. Normotensive rats exhibit regular oscillations in their tubular pressure. From Fig. 4.9 one can see that the modulation frequency of the fast myogenic oscillations (white circles) is in the same frequency band as the frequency of the TGF-mediated oscillations (black circles).

The tubular pressure data from a hypertensive rat (Fig. 4.10) are strongly nonstationary. All frequencies identified in the process show essential temporal variations (Figs. 4.10b, c and d). Despite this nonstationarity the proposed double-wavelet approach allows us to obtain a qualitative similarity between the dependences of the instantaneous modulation frequencies and the slow rhythm. Note, that "switchings" of the modulation frequencies take place earlier than the corresponding changes of the TGF dynamics. This may be a result of the averaging effect: To estimate the characteristics at a fixed time moment we use a "sliding window" with the width of the wavelet "mother" function at the chosen frequency, i.e. both some previous and some future dynamics are considered.

The analyses of experimental data presented to this point were made from tubular pressure recordings. Such measurements are rather easy to perform, and have relatively low measurement noise. They suffer from the disadvantage that the myogenic oscillations originate in the arterioles and that the fast oscillations

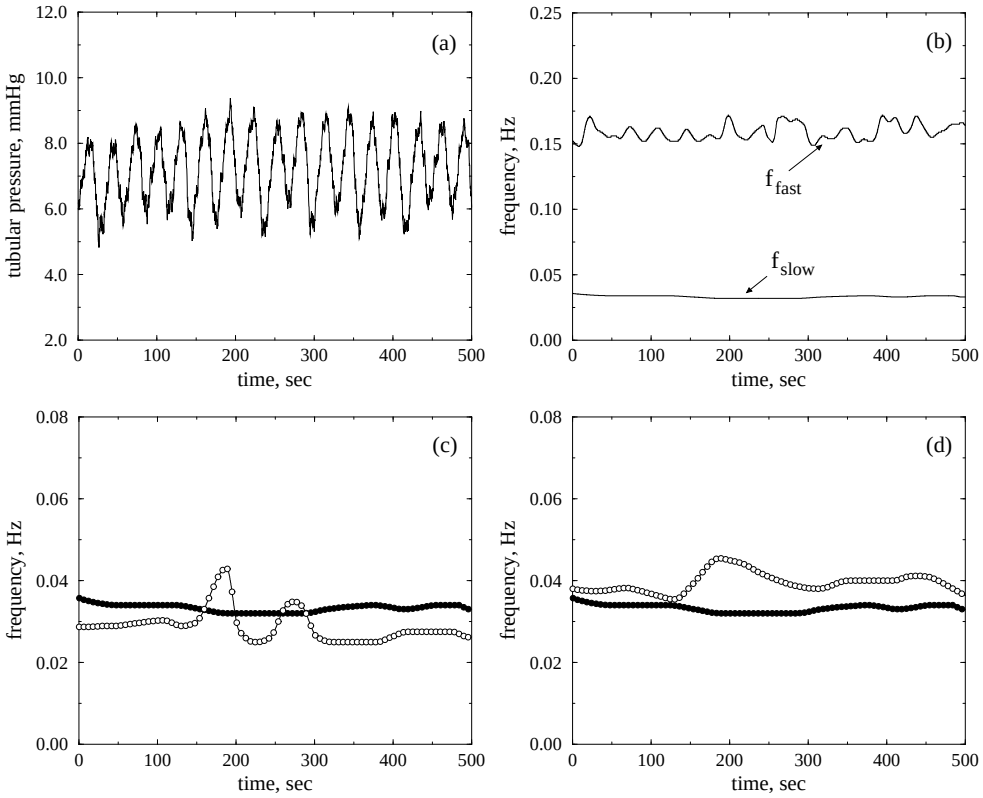

Figure 4.9: Experimental recording of the proximal tubular pressure in a single nephron of a rat kidney (a) and the extracted frequencies of rhythmic components (d). The search for f_{slow} and f_{fast} was performed in the ranges [0.02-0.07] Hz and [0.1-0.25] Hz, respectively. The frequency step in the wavelet transform was chosen to be 0.001 Hz. Results of the double-wavelet analysis: (d) and (c) correspond to the cases of frequency and amplitude modulation, respectively. Black circles mark $f_{slow}(t)$ and white circles indicate the instantaneous modulation frequency.

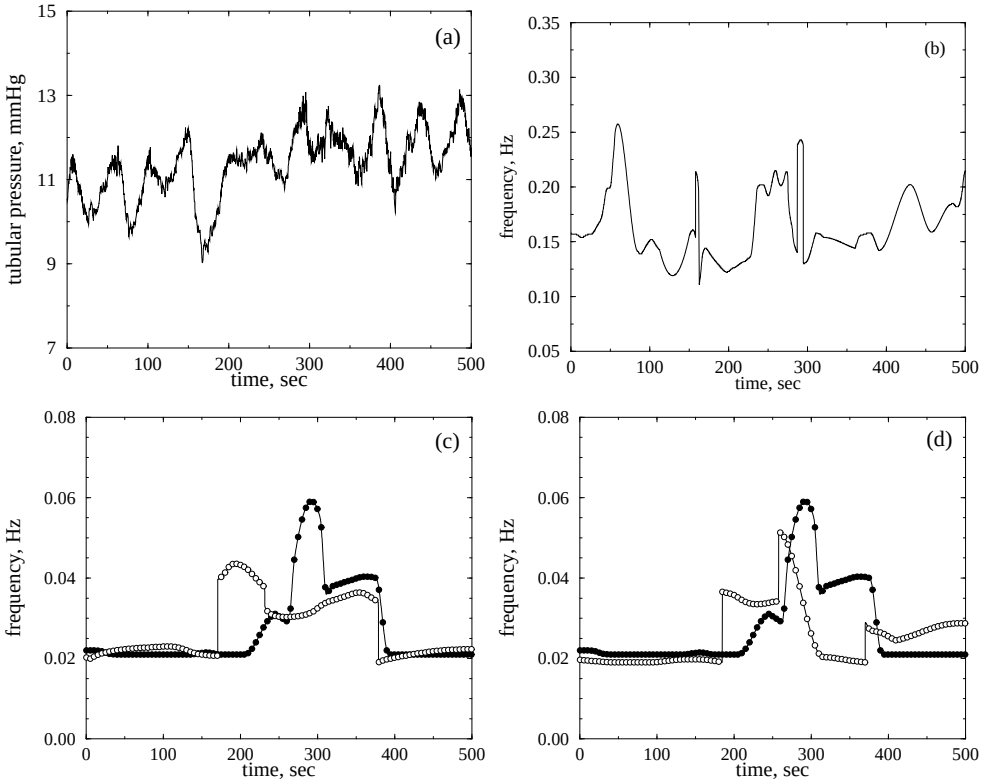

Figure 4.10: Analysis of the tubular pressure data for a hypertensive rat. (a) is the original time series. (b) demonstrates the instantaneous frequency of the fast mode $f_{fast}(t)$. (c) and (d) show the instantaneous frequency of the slow mode (black circles) and the modulation frequency (white circles) for the frequency and amplitude modulation of the fast mode, respectively.

in tubular pressure are damped by the compliant nature of the tubule wall, which (together with the associated flow resistances) serves as a mechanical low pass filter. An experimental laser Doppler method for measuring blood flow in a single efferent arterioles on the surface of the kidney (Smedley et al., 1993; Yip et al., 1993) allows one to observe more pronounced myogenic oscillations compared to those revealed by the tubular pressure recordings, but at the same time contain more measurement noise. At the level of whole kidney blood flow, a Volterra-Wiener kernel analysis has previously revealed nonlinear interactions between the two mechanisms in kidneys subjected to broad band forcing of the arterial blood pressure (Chon et al., 1994).

Figures 4.11 and 4.12 demonstrate the results obtained for a normotensive and a hypertensive rat, respectively. In both figures black circles denote the temporal dependences of the instantaneous frequencies of the slow oscillatory mode, and white circles are related to the instantaneous modulation frequencies. For a normotensive rat (Fig. 4.11) the modulation frequency displays some fluctuations around the frequency of the slow oscillatory mode. The variations from the TGF-frequency do not exceed 0.01 Hz, which is about the limit of detection of the method.

A similar situation exists for the hypertensive rat (Fig. 4.12), although the analyzed data are rather nonstationary. Some delay between the instantaneous frequencies (Fig. 4.12b) may arise from the above mentioned averaging effect. The modulation frequencies in Figs. 4.12c,d are close to the slow rhythm, although the rapid changes of the TGF-mode (around $t \approx 400$ sec) are not reproduced.

The depth of modulation also changes with time (Fig. 4.13). However, some averaged quantity can be used to characterize the dynamics. For the normotensive rat $M_f \approx 0.3$, while for the hypertensive rat $M_f \approx 1.1$. These results allow us to state that we observe a significant frequency modulation. Analogous studies can be performed for the instantaneous amplitudes of the fast mode. In this way, we obtained the values $M_a \approx 0.33$ and $M_a \approx 0.55$ (for the normotensive and the hypertensive rat, respectively), i.e., the effect

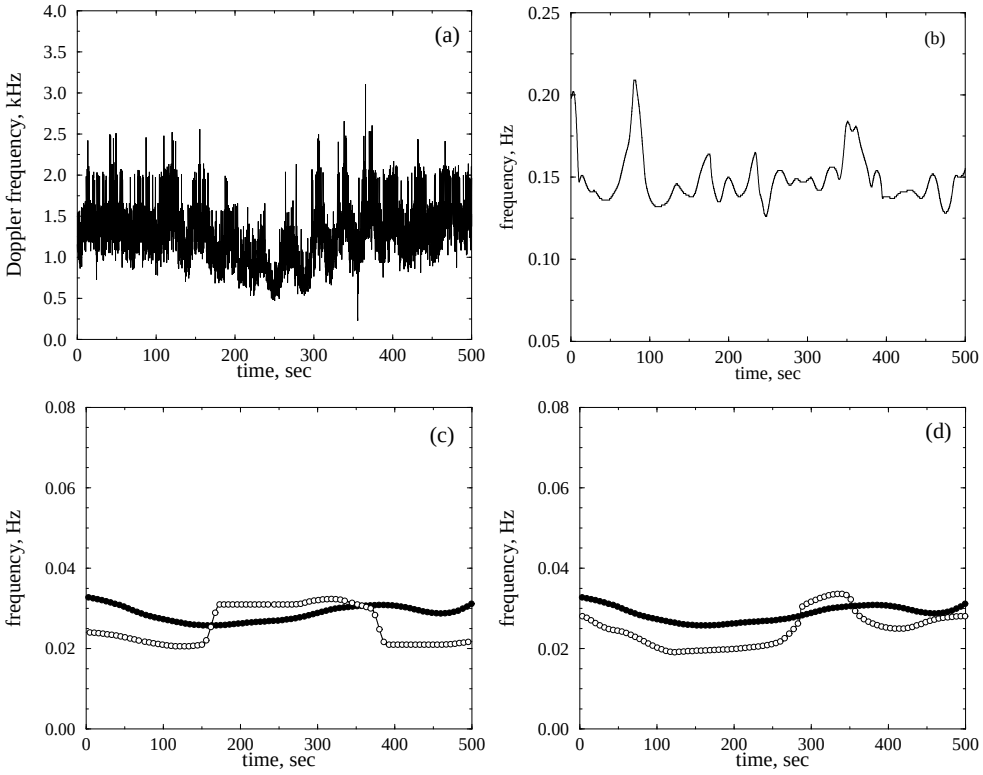

Figure 4.11: Analysis of blood flow data from the nephron of a normotensive rat. (a) is the original time series. (b) illustrates the instantaneous frequency $f_{fast}(t)$. (c) and (d) show $f_{slow}(t)$ (black circles) and the modulation frequency (white circles) for the frequency and amplitude modulation of the fast mode, respectively.

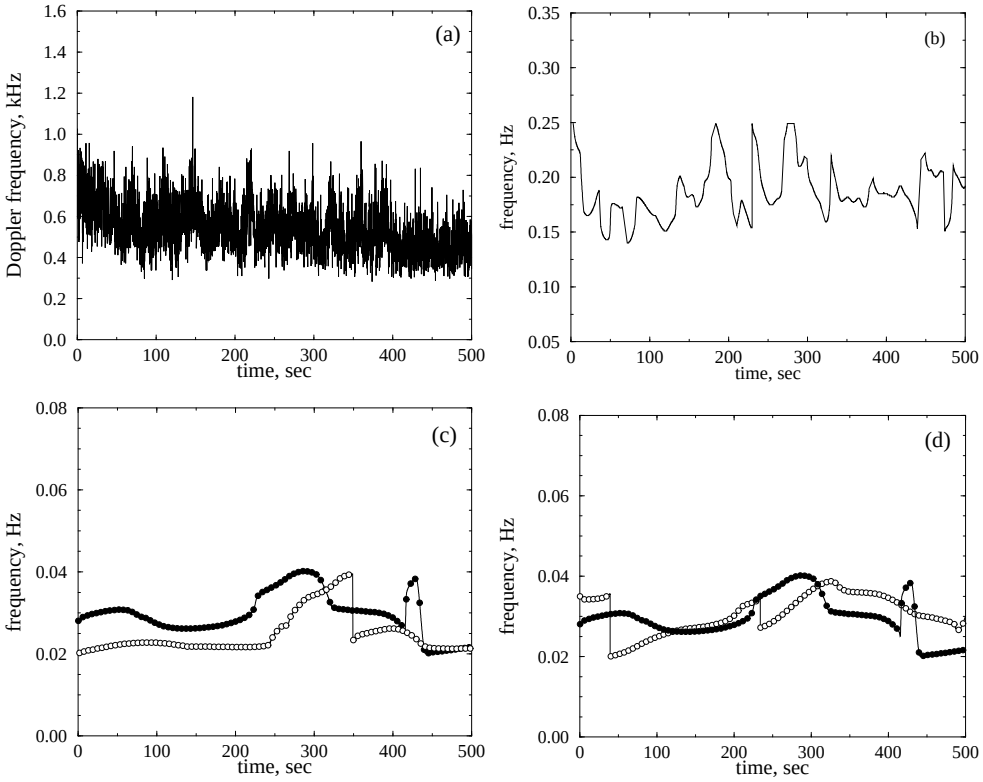

Figure 4.12: Analysis of blood flow data from a nephron of a hypertensive rat (a) exhibiting chaotic dynamics. The instantaneous frequency $f_{fast}(t)$ is shown in (b). (c) frequency modulation and (d) amplitude modulation. The extracted modulation frequencies (white circles) correspond to the frequencies of the slow mode (black circles).

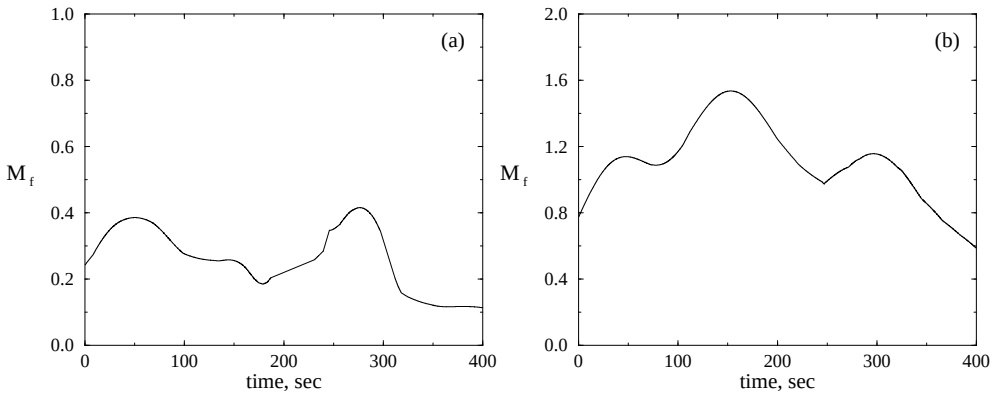

Figure 4.13: Time dependences of the depth of frequency modulation for a normotensive (a) and a hypertensive (b) rat. Note the significant difference in modulation depth between the two strains.

of amplitude modulation is less expressed than the frequency modulation from the viewpoint of absolute values of modulation depths. This observation may provide an important testing criterion for alternative models of the interaction between the two modes.

Statistical approach

Let us now discuss the results obtained for a series of experiments. We used 76 recordings, among which 34 were from normotensive rats and 42 were from hypertensive rats. Animal preparation and experimental procedure are described Section 1.3.

Figure 4.14 presents histograms of the instantaneous ratio of the modulation frequency to the TGF frequency at each moment of time over all recordings. It is clearly seen that there is a maximum around a ratio of unity. The width of the histogram may be related to different sources of variation in the system that are not normally distributed (the blood pressure, for example).

Figure 4.15a illustrates the distribution of depths of frequency and amplitude modulation for hypertensive (black circles) and normotensive (white circles) rats. Inspection of the figure clearly shows that there is a well-defined line of distinction between the two strains for both the amplitude and the frequency modulation, although the latter effect is more clearly expressed. Over

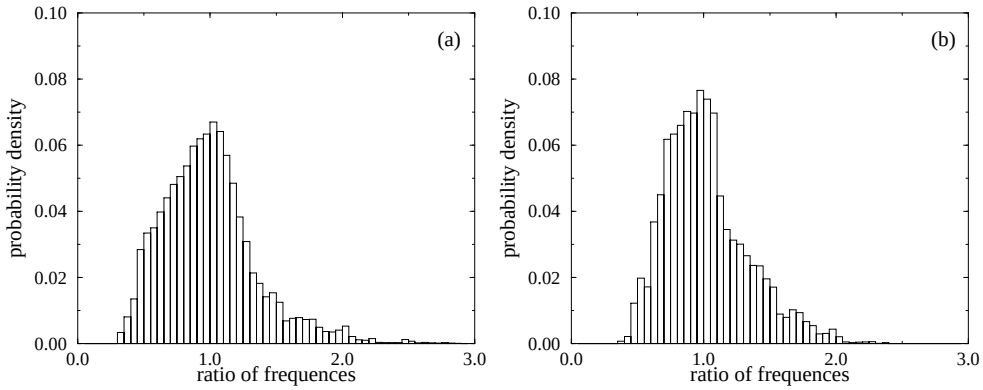

Figure 4.14: Distributions of the ratio of instanteneous frequencies as obtained from 76 experimental tubular pressure recordings. (a) Ratio of the frequency of amplitude modulation and (b) of the frequency of frequency modulation to the frequency of the slow TGF mode.

all data the mean values of the modulation depth with standard error of the mean are $M_a = 0.49 \pm 0.02$ and $M_f = 1.08 \pm 0.06$ as indicated by the dashed lines in Fig. 4.15a. It is clearly seen that the depth of modulation and, hence, the nonlinear interaction between the involved mechanisms, is stronger for hypertensive than for normotensive rats. The mean values are $M_a = 0.40 \pm 0.02$ and $M_f = 0.74 \pm 0.06$ for normotensive rats, while $M_a = 0.55 \pm 0.02$ and $M_f = 1.35 \pm 0.06$ for hypertensive rats. Figures 10b,c show the distributions of nephrons for the two rat strains according to their depth of frequency (Fig. 4.15b) and amplitude (Fig. 4.15c) modulation estimated from tubular pressure recordings. The number of nephrons with a frequency modulation that exceeds the average value is higher for hypertensive rats (75%) than for normotensive rats (18%). For the amplitude variations, we obtained 64% and 21%, respectively. The smaller difference between the amplitude modulations may be connected with the smaller values of M_a in comparison with M_f and, therefore, with the possible existence of spurious effects that influence our estimations for the amplitudes.

Based on the above results we suggest that the mechanism of regulation of the afferent arterial blood flow is more complex than previously assumed. In hypertension, the active parts of the blood vessels demonstrate increased

variability in their oscillations, i.e. regulation of the flow is associated not only with changes in vascular diameters but also with an accompanying adjustment of the frequency of the vascular oscillations.

Simulation

With the single nephron model we can demonstrate the possibility of extracting information about the modulation properties of the fast oscillatory mode from the slow phase variable P_t. For this purpose we consider two different dynamical regimes, namely periodic oscillations for $\alpha = 26$ and chaotic oscillations for $\alpha = 28$ (Fig. 4.16a,c). To show the efficiency of the proposed approach in the case of nonstationary dynamics we have performed a stepwise change of a selected control parameter: The parameter P_a characterizing the arterial pressure is changed from $P_a = 13$ kPa to $P_a = 13.3$ kPa at t=300 sec for the signal shown in Fig. 4.16a, and the parameter α is changed from $\alpha = 28$ to $\alpha = 31$ at the same time moment for the process considered in Fig. 4.16c.

Various tests performed with the nephron model in Chapter 2and with different simpler examples of modulation (such as a multiplicative interaction modeled by two harmonic functions) have shown that the presence of a slow nonstationarity, such as a variation of the arterial blood pressure with its $1/f$-spectral properties, does not have an essential influence on our ability to estimate the modulation frequency.

The results of our numerical investigations are presented in Figs. 4.16b and d. Here, the solid curves correspond to the instantaneous frequencies of the slow oscillatory mode. The instantaneous frequencies of the amplitude modulation (dashed) and of the frequency modulation (dotted) are obtained with the double-wavelet analysis. Note, that the modulation frequencies demonstrate a stronger floating around the slow rhythm in the chaotic regime. These fluctuations can probably be reduced by taking longer data with a better resolution. We decided, however, to restrict our findings to time series of the same length as available in our typical experimental recordings (4096 points).

Based on these results it is possible to conclude that (i) the proposed ap-

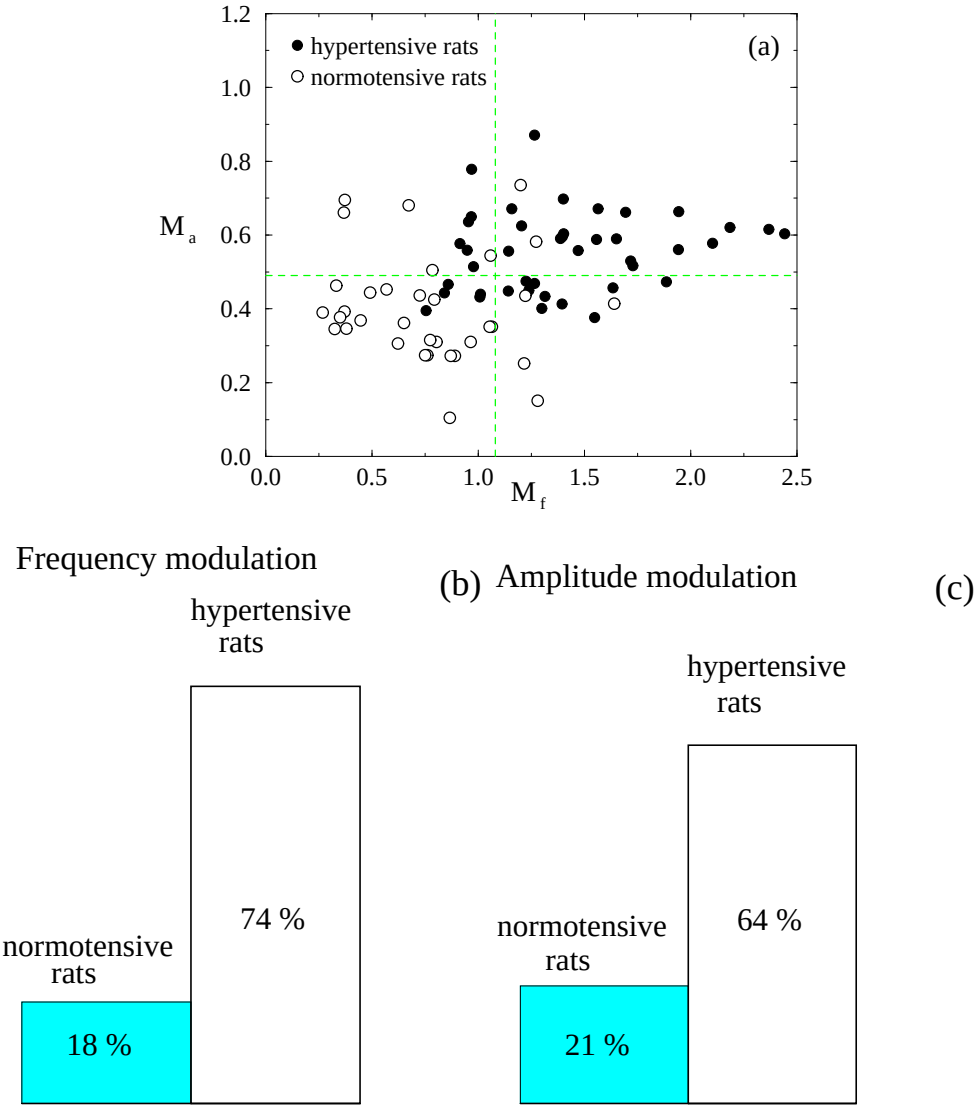

Figure 4.15: (a) Distribution of depths of frequency and amplitude modulation estimated from recordings of tubular pressure for normotensive rats (34 time series) and hypertensive rats (42 time series). Dashed lines represent the average values of the two modulation depths. (b) and (c) Fraction of nephrons with depth of frequency and amplitude modulation, respectively, that exceeds the average value over all experimental data of tubular pressure.

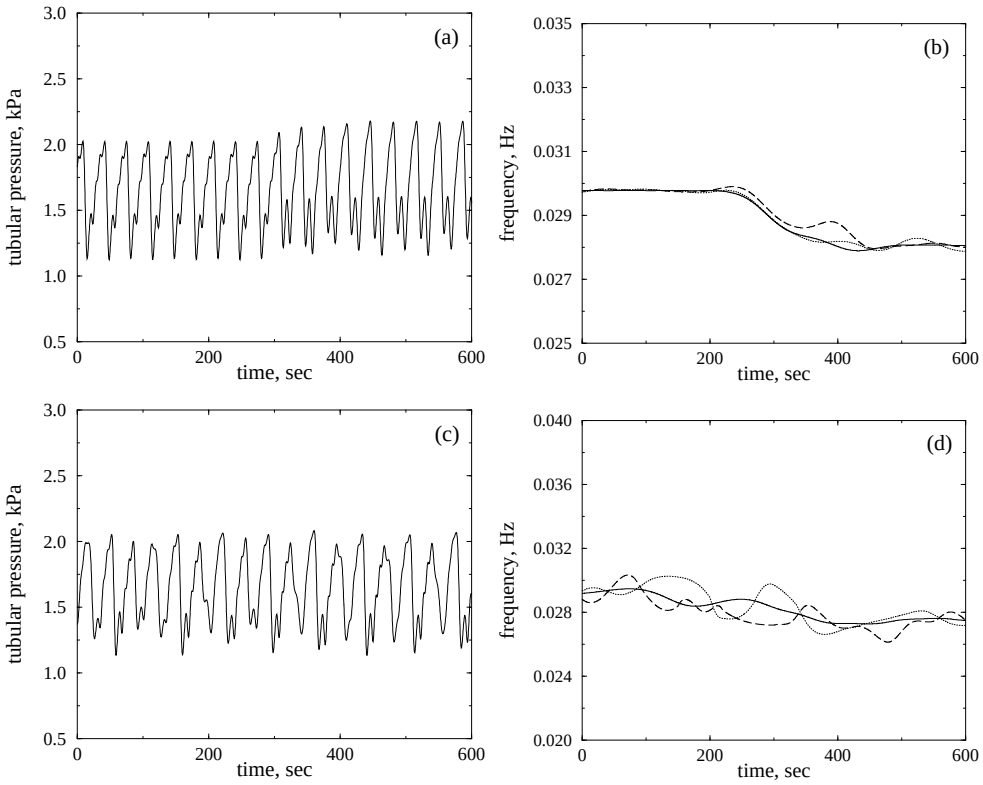

Figure 4.16: Numerical analysis of the mathematical model of a single nephron. Responses to a parameter change of the tubular pressure and modulation properties in the periodic (a,b) and chaotic (c,d) regimes, respectively. Solid curves in (b,d) correspond to the instantaneous frequency of the slow mode. The instantaneous modulation frequencies are presented by dashed curves (the case of amplitude modulation) and by dotted curves (the case of frequency modulation).

proach allows one to estimate the properties of modulation of the fast oscillatory mode extracted from the original miltimode data; and (ii) in accordance the model, both amplitude and frequency modulation are presented in the experimental data.

4.2 Synchronization between nephrons

4.2.1 Cooperative behavior

In Fig. 4.17 the left panel shows an example of different types of synchronization. Branching from different arterioles the nephrons in the two top traces operate nearly 180° out of phase. We consider anti-phase synchronization to be the signature of a strong hemodynamic component in the coupling, i.e., contraction of the afferent arteriole for one nephron causes the blood flow to the adjacent nephron to increase. In line with this interpretation, inspection of the arteriolar tree has shown that the nephrons in this case, while sharing an interlobular artery, are too far apart for the vascularly propagated coupling to be active. It is clearly seen, however, that the nephrons in the lower two traces, branching from the same arteriole, demonstrate in-phase synchronization.

Inspection of the right panel of Fig. 4.17 reveals that the three nephrons (all from the same arteriole) are synchronized and remain nearly in phase for the entire observation period (corresponding to ten periods of oscillation).

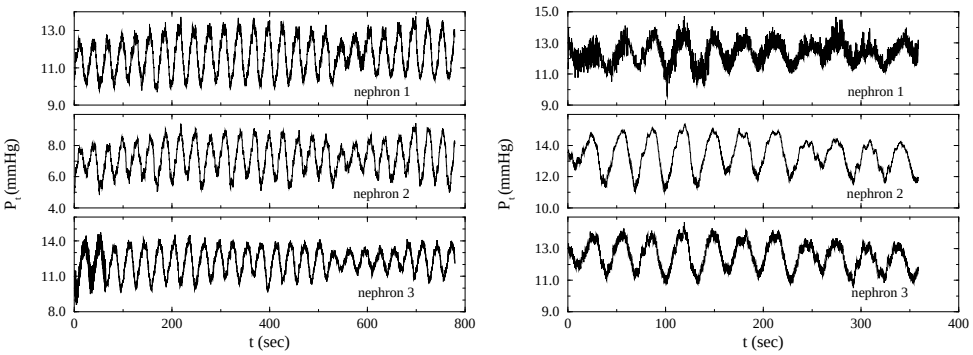

Figure 4.17: Simultaneous tubular pressure variations for a triple of coupled nephrons in two normotensive rats. The left panel demonstrates in-phase and anti-phase synchronization in the pressure variations between nephrons that belong to the same, respectively to different, arterioles.

Figure 4.18a shows variations of the (normalized) phase difference for the regular pressure variations in a normotensive rat. One clearly observes in-phase ($\Delta\phi \cong 0$) and anti-phase ($\Delta\phi \cong \pi$) synchronization for nephrons branching from the same and from different arterioles, respectively. All three nephrons

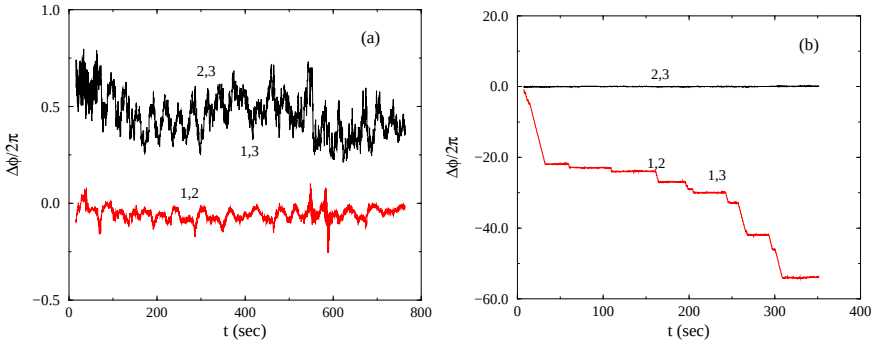

Figure 4.18: Relative phase dynamics for pairs of nephrons in normotansive rats. (a) illustrates in phase ($\Delta\pi \approx 0$) and anti-phase synchronization ($\Delta\pi \approx 0.5$) for nephrons with dominating vascularly propagated and hemodynamic coupling, respectively. (b) shows the variation of the phase difference for nephrons branching off from the same arteriole.

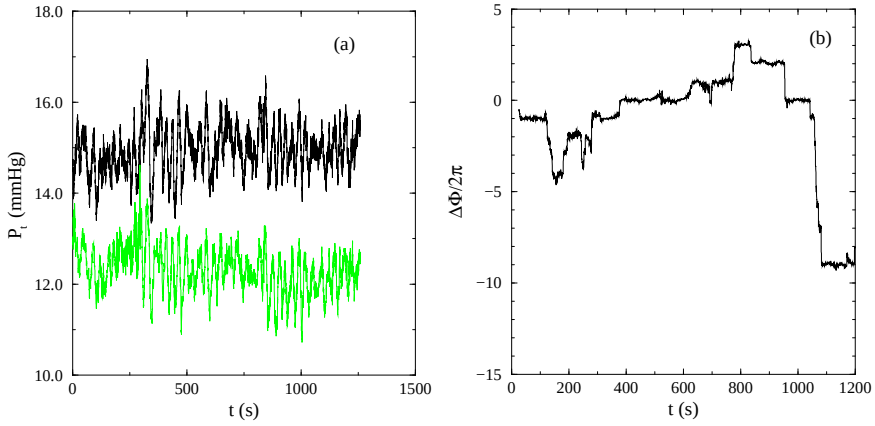

Figure 4.19: (a) Example of the tubular pressure variations that one can observe in adjacent nephrons for hypertensive rats and (b) variation of the normalized phase difference $\Delta\phi/2\pi$ for the irregular pressure variations. This is an illustration of the phenomenon of chaotic phase synchronization.

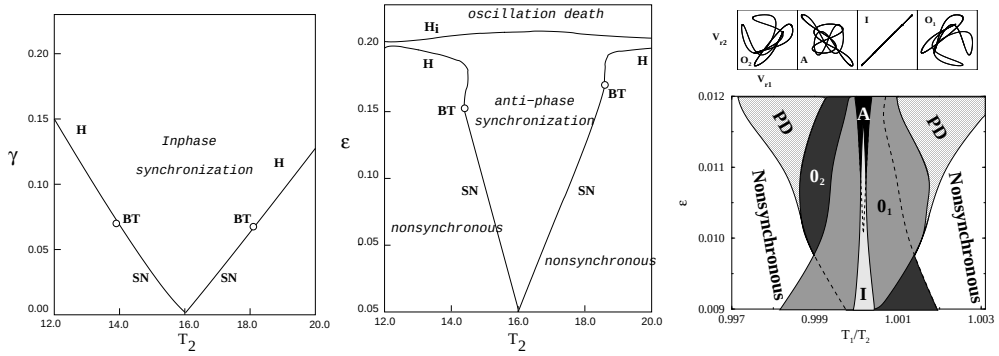

Figure 4.20: Interplay between vascular propagating and hemodynamic coupling. (a) In-phase synchronous regime observed for pure vascular propagating coupling. (b) Anti-phase synchronous regime observed for pure hemodynamic coupling (c) Synchronization regions for coexisting families of attractors ($\gamma = 0.004$). $\alpha = 18.595$, $T_2 = 16.0$ s

in the triple (b) demonstrate synchronous behavior but there are characteristic phase slips of 2π (or an integer number of 2π) because of the noisy conditions under which the nephrons operate.

Figures 4.19 represents an example of the tubular pressure variations in pairs of neighboring nephrons for hypertensive rats. These oscillations are significantly more irregular than the oscillations displayed in Figs. 4.17 and, as previously discussed, it is likely that they can be ascribed to a chaotic dynamics. In spite of this irregularity, however, one can visually observe a certain degree of synchronization between the interacting nephrons. The normalized phase difference $\Delta\Phi/2\pi$ for the irregular pressure oscillations in Fig. 4.19b reveals characteristic locking intervals with intermediate phase slips. Here, we note the interval from $t \cong 400$ s to $t \cong 800$ s (corresponding to 16 oscillations of the individual nephrons) where the phase difference remains nearly constant.

We conclude that the experimental results show clear evidence of synchronization of neighboring nephrons both for normotensive and for hypertensive rats. Moreover, one can observe both in-phase and anti-phase synchronization, associated, presumably, with two different coupling mechanisms between the nephrons.

Simulation

Figure 4.20 shows a segment of the bifurcation diagram for synchronous solutions on the mismatch *vs.* coupling parameter plane. With variations of coupling trength of the vasculary propagated and hemodynamic interactions different dynamical regimes can take place: in-phase for pure vascular propogating coupling, anti-phase for pure hemodynamic coupling, and out-of-phase solutions when both interactions take place.

The individual oscillatory system has two modes that can be locked with each other. However, an interaction between functional units can break their mutual adjustment. It is also plausible that a coupling can act in different manners on the fast and slow oscillations. For the interacting systems we introduce two rotation numbers as follows:

$$r_v = T_{v1}/T_{v2}, \quad r_h = T_{h1}/T_{h2}. \tag{4.4}$$

To provide more information, the variation of the phase difference is calculated separately for the slow h and for the fast v oscillations.

Let us consider the case of $\alpha = 30.0$ corresponding to a weakly developed chaotic attractor in the individual nephron. The coupling strength γ and delay time T_2 in the second nephron are varied. Two different chaotic states can be recognized as asynchronous and synchronous (Fig. 4.21). For asynchronous behavior the rotation numbers r_h and r_v change continuously with T_2 while inside the synchronization region two cases can be distinguished. To the left, the rotation numbers r_h and r_v are both equal to unity since both slow and fast oscillations are synchronized. To the right ($T_2 > 14.2$ *sec*), while the slow h-mode of the chaotic oscillations remain locked, the fast v-mode drifts randomly. In this case the synchronization condition is fulfilled only for one of oscillatory modes.

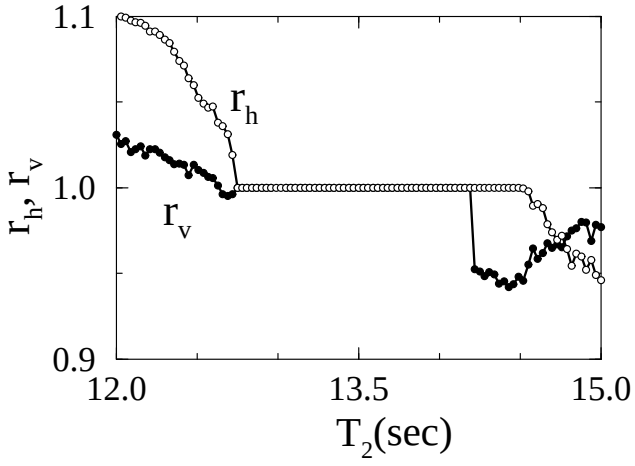

Figure 4.21: Full and partial synchronization of fast and slow motions ($T_1 = 13.5$ *sec*, $\alpha = 30.0$ and $\gamma = 0.06$). The simulation results depicted in this figure reproduce all the different experimental results observed in the wavelet analysis.

4.2.2 Comparison of normotensive and hypertensive rats

Frequency and phase synchronization are useful alternate approaches to evaluating entrainment in phenomena in coupled systems . The two approaches are not identical because frequency synchronization characterizes the average behavior of a system over some time interval while phase synchronization describes the system at each time moment and provides additional information on phase shifts. For chaotic and stochastic systems these two approaches can give different results.

Frequency entrainment

We shall refer to those pairs that had origins from the same cortical radial artery as neighbouring nephrons. Figure 4.22 illustrates two different synchronization states that can occur in a pair of neighbouring nephrons. In Fig. 4.22a the ratio $f_1(t)/f_2(t)$ between the frequencies in the two nephrons remain close to 1:1 throughout the observed time interval for both the slow and the fast modes. One can observe some fluctuation in the frequency ratio, particularly for the fast modes, but the amplitude of this fluctuation remains within a limit of $\pm 10\%$ of the nominal frequency. In Fig. 4.22b, on the other hand, the only

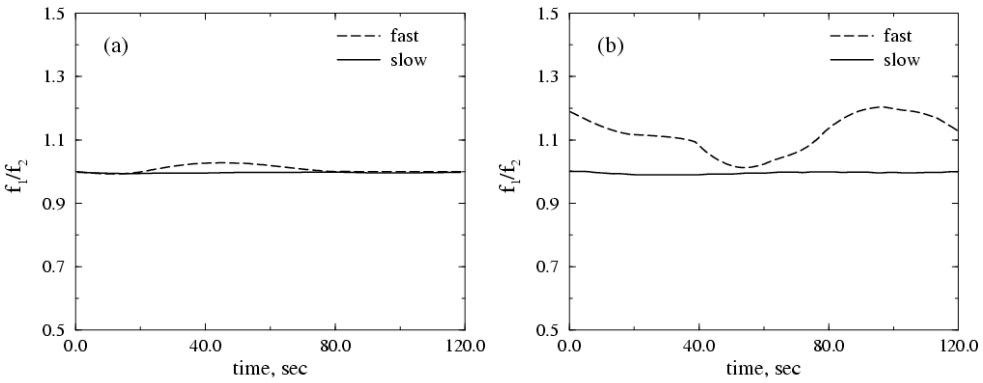

Figure 4.22: Bimodal (a) and partial (b) coherence in the dynamics of paired nephrons for a normotensive and a hypertensive rat, respectively.

synchronization between the two nephrons is in the slow mode. The frequency ratio of the fast mode varies over the time course of the experiment, exceeding the 10% limit for more than half the observation time, and does not settle at a plateau at or near 1.00. Figure 5b illustrates a case of partial synchronization.

For each pair of experimental data series we determined the time intervals where the modulus of the difference between the corresponding instantaneous frequencies did not exceed a predetermined fixed value. The oscillations are synchronous in these intervals. We have chosen the limits of the synchronous dynamics to be $\pm 10\%$ of the value of the mean instantaneous frequency: ± 0.003 Hz for the slow mode and ± 0.015 Hz for the fast mode. Other limits produce similar results, except that a widening of the limits results in longer locking times; the qualitative picture, and in particular the distinctions between two rat strains remains the same.

As shown in Table 1, there is a difference in synchronization phenomena between the normotensive and the hypertensive rats. Nephrons of normotensive rats supplied from the same cortical radial artery are fully coherent 81% of the time, where both the slow and the fast oscillations synchronize as seen in Fig. 4.22a. The other combinations of possible dynamics have a significantly lower probability of occurrence. In contrast the most probable state for the hypertensive rats is one of partial synchronization where either the slow or the fast rhythms are locked while the other mode remains non-synchronous, as seen

in Fig. 4.22b. The slow mode locks more frequently than the fast mode.

	Probability, %	
Type of dynamics	Normotensive rats	Hypertensive rats
bimodal coherence	81	39
complete incoherence	0.4	16
partial coherence:		
(only for slow rhythms)	13	36
(only for fast rhythms)	6	10

Table 1. Probability of different combinations of frequency entrainment in tubular pressure measurements from 9 pairs of nephrons in normotensive rats and 11 pairs of nephrons from hypertensive rats.

Figure 4.23 shows the probability of finding different time intervals of coherent dynamics. In normotensive rats, the slow TGF mediated oscillations have a probability of 40% of remaining synchronized longer than 250 s, a duration that represents 8 or more periods of the oscillation. For hypertensive rats that probability is only 12%. Fast myogenic oscillations similarly have a probability of about 30% of remaining synchronized for more than 50 s, corresponding to 8 periods of the myogenic oscillations, while for hypertensive rats this probability is only 12%. Slow oscillations in normotensive rats are 3-4 times as likely to display long locking times as in SHR, and a similar factor applies to the fast oscillations.

The mean locking times, under the condition that effective synchronization is defined as a frequency change less than $\pm 10\%$ of the mean instantaneous frequency, were 360 ± 31 s and 75 ± 14 s for the slow and the fast dynamics in normotensive rats; the corresponding locking times for SHR were 100 ± 16 s and 25 ± 4 s, respectively. The differences between normotensive rats and SHR were highly significant for both the slow mode (P=0.00003) and the fast mode (P=0.00015). We conclude that the hypertensive rats demonstrate significantly shorter intervals of coherent dynamics than normotensives.

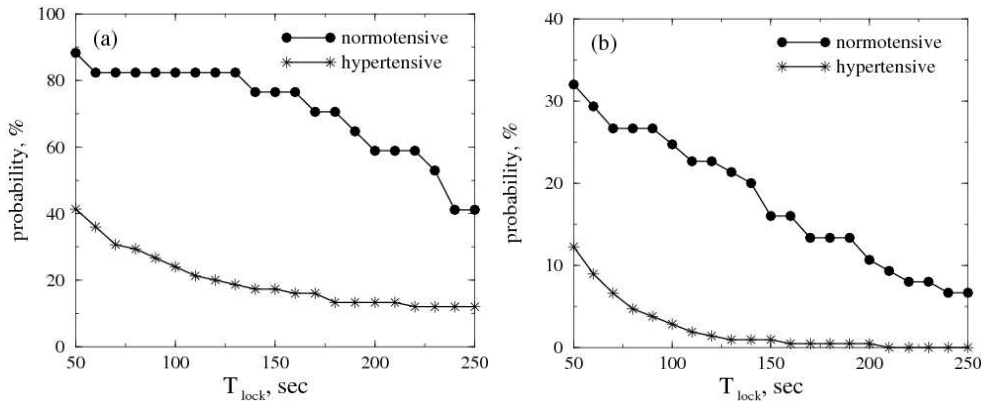

Figure 4.23: Probability of finding intervals of frequency locking that exceed for the slow (a) and the fast (b) dynamics. This probability was estimated by calculating the relative number of time series that contain locking intervals larger than . Two data records from normotensive rats and one SHR that were shorter than 600 sec were not analyzed for this figure.

We also analyzed data from paired nephrons that were found to originate from different cortical radial arteries. In these measurements we expected to find no interaction because of the origin from different cortical radial arteries, and visual inspection of the original data confirms this expectation. For normotensives the slow oscillation had a mean locking time of 48 ± 5 s and the fast oscillation 27 ± 4 s; for hypertensives the corresponding findings were 42 ± 6 s and 15 ± 2 s. The estimated locking time of these TGF oscillations is less than 2 full periods. The results confirm the prediction and also the specificity of the analytical methods.

Phase entrainment

As in the case of frequency adjustments we need to formulate the conditions under which the dynamics can be considered as synchronous. For 1:1 synchronization, this condition should ensure that the modulus of the phase difference between the oscillations in the paired nephrons does not exceed some fixed value γ. Here, we have chosen $\gamma = 2\pi/10$ for the slow rhythm and $\gamma = 2\pi/6$ for the fast mode. The time series we analyzed are neither stationary nor free of noise, and these factors can cause some variability in the phase angle difference. The

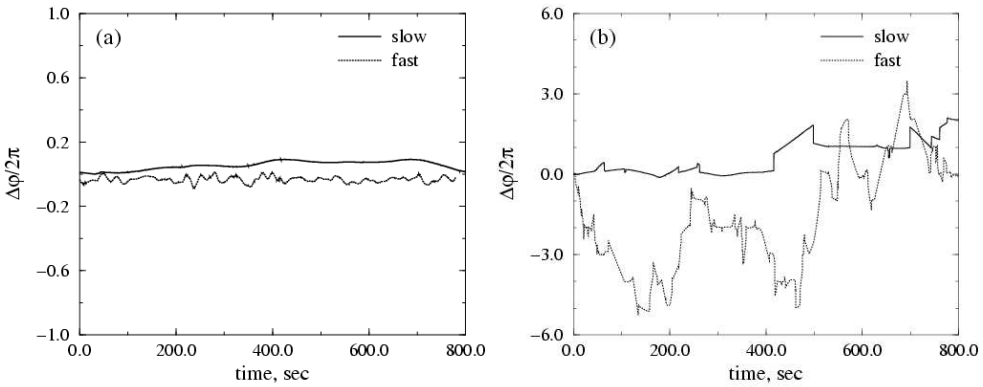

Figure 4.24: Phase differences for the slow and the fast oscillations of paired nephrons obtained from a normotensive (a) and a hypertensive (b) rat. Note the different vertical axes used in (a) and (b).

values of γ we chose allow for some variability from these sources. The different values of γ account for a significantly higher variability of the myogenic oscillations. The duration of the mean locking time, our measure of the degree of synchronization, depends on the condition applied to the parameter γ, but even with different conditions for γ the qualitative synchronous patterns remain the same.

Figure 4.24a shows variations of the normalized phase difference for the regular pressure dynamics in a normotensive rat; the synchronization of the slow and the fast oscillations for nephrons branching from the same cortical radial artery is apparent. Nephron dynamics of a hypertensive rat, shown in Fig. 4.24b, are more complicated, especially with respect to entrainment of the myogenic components. It is possible to find examples where the fast modes demonstrate segments of the phase-locked oscillations, although a more typical case is when the phase-locked regime occurs only for short time intervals. Figure 4.24b illustrates partial entrainment because only the slow mode demonstrates intervals of phase-locked dynamics for a longer duration than a single period of the slow oscillations, which is about 30 s.

Table 2 shows the probabilities of finding different states of phase-synchronized dynamics. The results are similar to those obtained with the frequency locking approach. The values given in Tables 1 and 2 can vary depending on the re-

strictions used for defining the synchronous state but they illustrate that paired nephrons in normotensive rats typically show full synchronization where all oscillatory modes are synchronized; nephrons in hypertensive rats often demonstrate partial entrainment. The total probability of observing partial synchronization, 41%, exceeds the probability of the full synchronization, 35%, and both types of partial synchronization are prominent.

	Probability, %	
Type of dynamics	Normotensive rats	Hypertensive rats
Bimodal synchronization	71	35
Nonsynchronous	5	24
partial coherence:		
(only for slow rhythms)	17	28
(only for fast rhythms)	7	13

Table 2. Probability of different states of phase synchronization in paired nephrons.

Distinctions in the appearance of large intervals of phase-synchronized dynamics are very similar to those presented in Fig. 4.23 confirming differences between normotensive and the hypertensive rats. The mean times of phase-locking were 270 ± 23 s and 60 ± 12 s for the slow and the fast oscillations in normotensive rats, and 90 ± 14 s and 20 ± 3 s, respectively, for SHR. The differences between normotensive rats and SHR were highly significant for both the slow mode (P=0.000001) and the fast mode (P=0.0014). Although these results are not exactly the same as those found for frequency entrainment, the relationships among them are similar and support the conclusion that the hypertensive rats have a shorter duration of synchronous dynamics and a higher probability of partial synchronization than their normotensive counterparts.

4.2.3 Vascular-coupled nephron tree

There are no experimental results on the dymanics of vascular-coupled nephron tree. Therefore we focus here on simulation results that can predict overall

behavior.

The model produced a mixture of steady state, quasiperiodic, and chaotic solutions for nephrons in the ensemble. The value of the tubule pressure in the steady state solutions varied with arterial pressure and the strength of nephron-nephron coupling. Figure 4.25 shows examples of phase plane projections of the quasiperiodic and chaotic solutions, together with the results of a simulation of a single nephron not a part of an ensemble. The results are shown as trajectories on the plane defined by the tubular hydrostatic pressure and the afferent arteriolar radius.

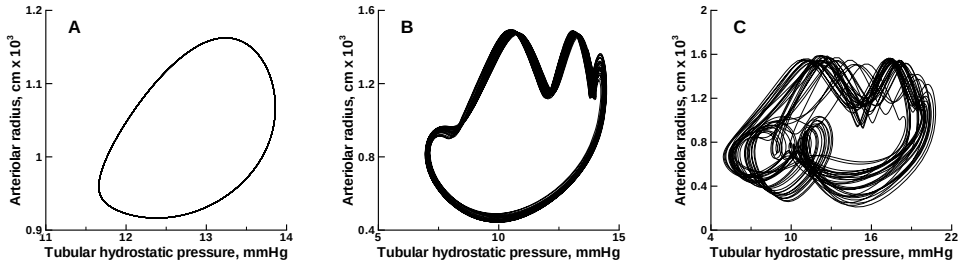

Figure 4.25: Phase plane plots of nephron model results. (a): a single nephron model, showing a limit cycle oscillation. (b): nephron 1 of the ensemble of 22, with arterial pressure at 100 $mmHg$ and θ, the strength parameter of nephron nephron coupling, at 0.5, showing quasiperiodic motion. (c): nephron 1, with arterial pressure at 125 $mmHg$ and θ at 1.0, showing a chaotic attractor. Each figure was obtained by simulating 5000 s.

Our results for a single nephron, shown in Fig. 4.25, are the same as have been reported previously (Barfred et al., 1996; Holstein-Rathlou et al., 2001). The tubule pressure and the arteriolar diameter oscillate, and the motion on the phase plane is that of a limit cycle oscillator. Parameters have been chosen that are typical of measurements made in normal animals. With these values, $\alpha = 12$ and arterial pressure 100 $mmHg$, the myogenic oscillations remain inactive in the dynamics of the uncoupled nephron. The value of $\alpha = 12$ was used for all simulations reported in this study. For higher values of the gain parameter α of the TGF mechanism, the individual nephron displays a combination of fast myogenic and slower tubuloglomerular oscillations and, as previously reported, one can observe the phenomena of intra-nephron synchronization, period-doubling

and transitions to chaos (Barfred et al., 1996; Sosnovtseva et al., 2002a).

The simulation of the nephrons that form the ensemble behaved differently in several respects. First, the amplitude of the tubular pressure fluctuation was greater in nephrons acting as part of the ensemble than in the single nephron, even though the parameter values were the same in the respective simulations. This result is analogous to the results in Ref. (Pitman et al., 2004) that the value of the bifurcation parameter needed to achieve the Hopf bifurcation in a single nephron model was reduced when two nephron models were coupled. Second, the simulations produced almost periodic behavior in many nephrons, but in no case was the motion strictly that of a limit cycle oscillator. As shown in Fig. 4.25b, one form of behavior showed quasiperiodicity, with two or more incommensurate frequencies.

A typical power spectrum from a nephron with quasiperiodic oscillations shows several peaks: three strong peaks associated with the TGF signal and its harmonics, peaks at higher frequencies arising from the myogenic oscillations and their harmonics, and a broader less pronounced peak at very low frequencies arising from the interactions in the nephron tree. Similar low frequency components have been observed in experimental spectra and ascribed to internephron coupling phenomena, presumably in the form of beating between the TGF oscillations in different nephrons or because of a new type of collective modes in the tree structure (Jensen et al., 1986).

For purposes of assessing synchronization we have compared only the frequencies of the TGF oscillation; we considered neither the fast myogenic oscillations nor the slower frequencies imposed by the ensemble. We implemented the model under two sets of conditions designed to permit study of different aspects of synchronization. To test the interaction among nephrons of different lengths we applied identical time delays to all cortical nephrons, and longer delays to the three groups of medullary nephrons, as described above. In the other set we added small random contributions to the time delay of each of the nephrons.

We first examined nephrons operating only in a quasiperiodic mode, which occurs at an arterial pressure of 100 $mmHg$ and a coupling parameter of $\theta = 0.5$.

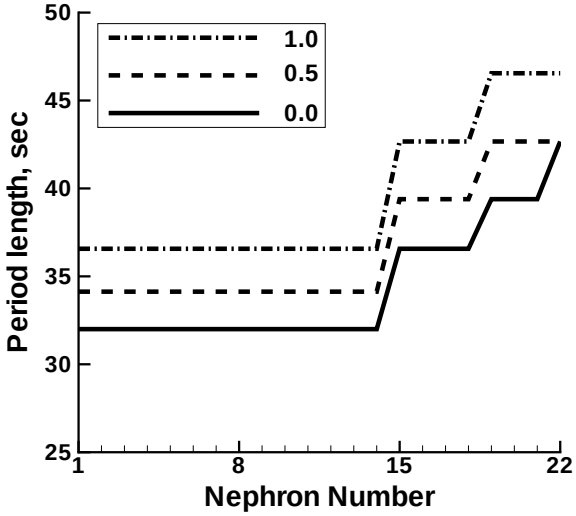

Figure 4.26: Period length vs nephron number, for 3 values of θ, the strength of coupling between nephrons. Arterial pressure: 100 $mmHg$.

These values are the normal arterial pressure and the value of θ measured experimentally in normotensive rats. Figure 4.26 shows the dominant period lengths for various values of the coupling strength. In the data set with no nephron-to-nephron coupling, the period lengths for cortical nephrons did not vary from nephron to nephron because the time delays were identical.

Increasing nephron-to-nephron coupling to encompass the range of physiologically measured values had several effects. Period lengths for all nephrons increased with coupling strength, and, as will be seen below, the amplitude of tubular pressure oscillations increased. Increased coupling also permitted synchronization among juxtamedullary nephrons with different time delays. Nephron 22 has a longer delay than any of the others, and has the longest period length when internephron coupling is set to 0. At higher values of the coupling strength, nephron 22 becomes entrained with nephrons 19-21 to form a cluster with a single frequency. The shorter juxtamedullary nephrons, numbers 15-18, all oscillate at a single frequency, which did not become entrained with either the cortical nephrons or the longer juxtamedullary ones. The model therefore predicts at least 3 distinct frequencies operating along a cortical radial

artery.

Next we altered the time delay in each of the 22 nephrons by adding a random number as described above. As shown in Figure 4.27, first panel, randomization of the time delays produces a set of time series without synchronization, so long as the coupling strength θ was 0. The juxtamedullary nephrons, numbers 15–22, had longer periods and larger oscillations than the cortical nephrons.

Figure 4.27, second panel shows the same array of nephrons as in Figure 4.27, upper panel, but with the value of θ set to 0.5, which falls within the renage of experimentally measured values, and that permits synchronization. The magnitude of the oscillations was greater with synchronization than without. There were phase differences among the shorter cortical nephrons, but all oscillated at the same frequency. The juxtamedullary nephrons did not synchronize with cortical nephrons. The introduction of variation in the time delays produced a more complex pattern of synchronization among the juxtamedullary nephrons and this pattern differed among the sets produced by different random number series. In all cases the cortical nephrons synchronized among themselves at a single frequency, but in no case did the juxtamedullary nephrons synchronize with the cortical nephrons.

Results with a parameter set selected to generate a chaotic time series in all nephrons, arterial pressure at $125 mmHg$ and $\theta = 1.0$, are shown in Figure 4.27, third panel. Although all 22 time series in this simulation showed attractors similar to those of Fig. 4.25c, the dominant frequency was that of the TGF oscillation, and each of the oscillations had the same frequency, demonstrating strong synchronization.

Figure 4.28, first panel, shows the pressures in the cortical radial artery from the same simulation shown in Figure 4.27, first panel, with no nephron-nephron coupling. The pressure drop was calculated using vessel length and radius data from Ref. (Nordsletten et al., 2006). There is a pressure drop of a few percent along the cortical radial artery as it distributes blood to the afferent arterioles, and there are minor oscillations in pressure. Figure 4.27, first panel shows the tubular pressure oscillations present in the nephrons associated

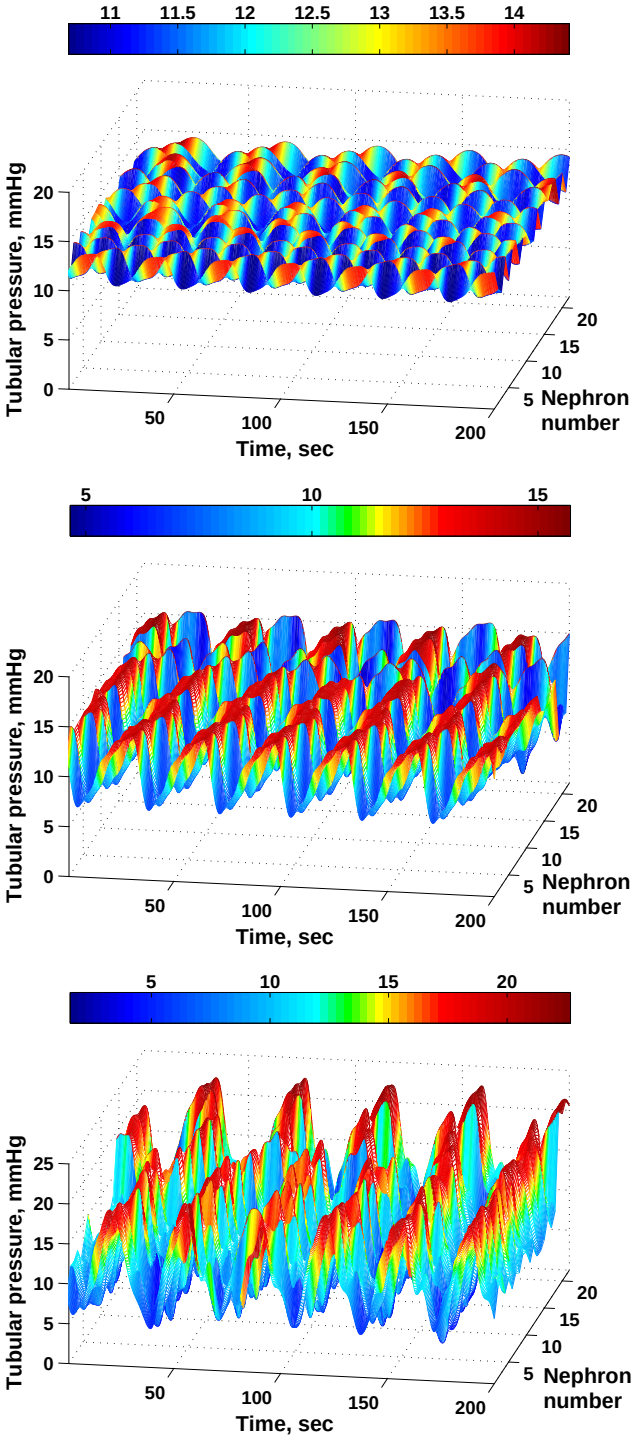

Figure 4.27: Tubular hydrostatic pressure in all nephrons of the ensemble. First panel: $\theta = 0$; arterial pressure: 100 $mmHg$. Second panel: $\theta = 0.5$; arterial pressure: 100 $mmHg$. Third panel: $\theta = 1.0$; arterial pressure: 125 $mmHg$. The bars show the color scales used to present the tubular pressures in the three panels.

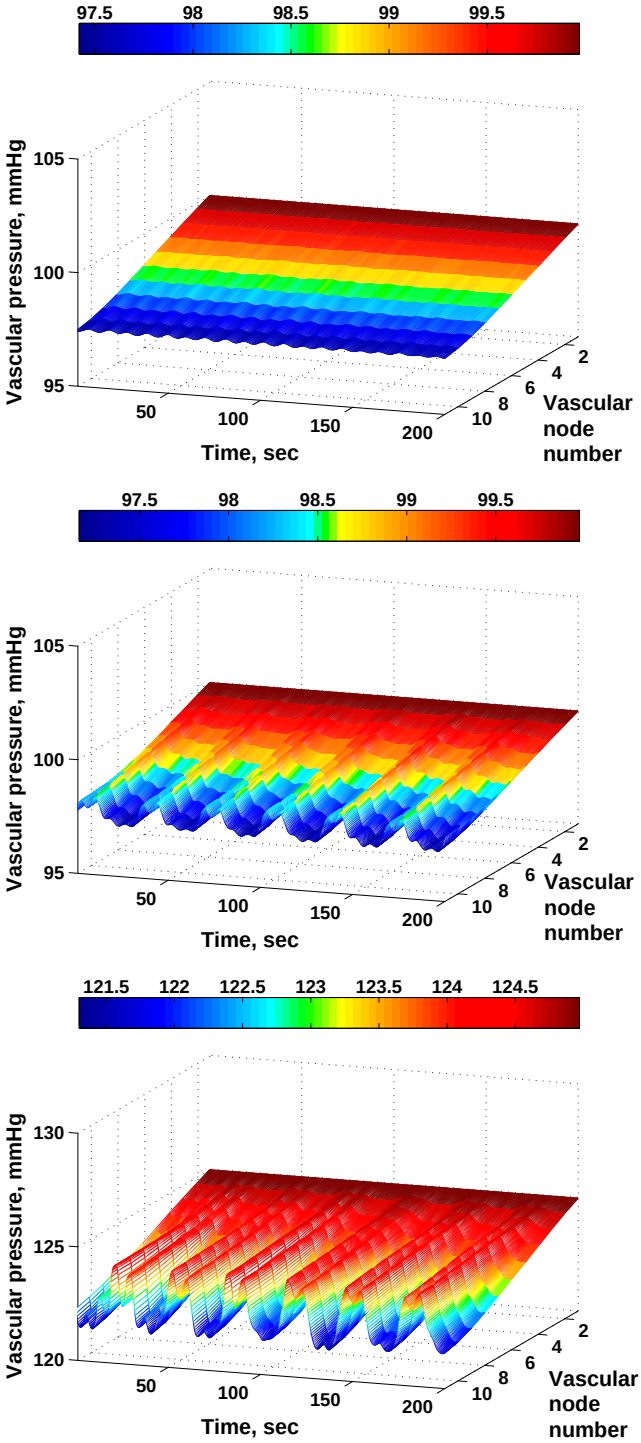

Figure 4.28: Vascular hydrostatic pressure in the model. Top panel: $\theta = 0$, arterial pressure: 100 $mmHg$. Middle panel: $\theta = 0.5$, arterial pressure: 100 $mmHg$. Lower panel: $\theta = 1.0$, arterial pressure: 125 $mmHg$.

with the vascular pressures in Figure 4.28, first panel. The tubular pressures remain unsynchronized. This result suggests that hemodynamic coupling is not functionally important under the present conditions.

Figure 4.28, second panel, shows vascular pressure results from the same simulation shown in Fig. 4.27, second panel, with nephron-nephron coupling active. When there is synchronization of nephron oscillations an oscillation in vascular pressure emerges at the same frequency as the synchronized oscillation of the cortical nephrons. There is an imperceptible oscillation of the vascular pressure supplying the longer juxtamedullary nephrons. These longer nephrons are supplied from the arcuate artery and the beginning of the cortical radial artery where the blood flow is higher than at the end of the cortical radial artery. Because the blood flow in the cortical radial artery near its beginning is large compared to the blood flow to the medullary nephrons, the oscillations in blood flow to these nephrons have only minor effects on vascular pressure. As blood flows toward the end of the cortical radial artery the blood flow rate drops and the effect of oscillations in afferent arteriolar resistance increase, leading to larger oscillations in vascular pressure.

Figure 4.28, third panel, contains the results of vascular pressure calculations in the data set of Fig. 4.27, third panel, that predicts chaotic tubular pressure trajectories. An oscillation in vascular pressure accompanies the oscillation in tubular pressures and flows, and in addition, the irregular fluctuations that give the tubular pressure time series their chaotic property produce similar irregularities in the vascular pressure record. The oscillation in vascular pressure shown in Figs. 4.28, second and third panels arise because of resource distribution by the network.

TGF and the myogenic mechanism work in the kidney to regulate blood flow to individual nephrons; the main perturbations come from the arterial pressure, which fluctuates with a $1/f$ pattern (Marsh et al., 1990; Holstein-Rathlou et al., 1995). We therefore exercised the model varying blood pressure over the range 90 $mmHg$ to 130 $mmHg$, and the coupling parameter θ from 0.0 to 1.5. We sought only to determine the main classification of dynamical activity over

these ranges. Figures 4.29a, b, and c present the results for nephrons 1, 15, and 22, respectively. Nephron 1 is the most superficial of the cortical nephrons and represents those on the surface of the kidney that have been submitted to experimental investigation. Nephron 15 is the shortest of the juxtamedullary nephrons; its dynamics have not been studied experimentally. Nephron 22 is the longest juxtamedullary nephron, and its dynamics have also not been studied experimentally. A single value of the seed for the random generator was used for all of the 3×110 simulations represented in Figure 4.29.

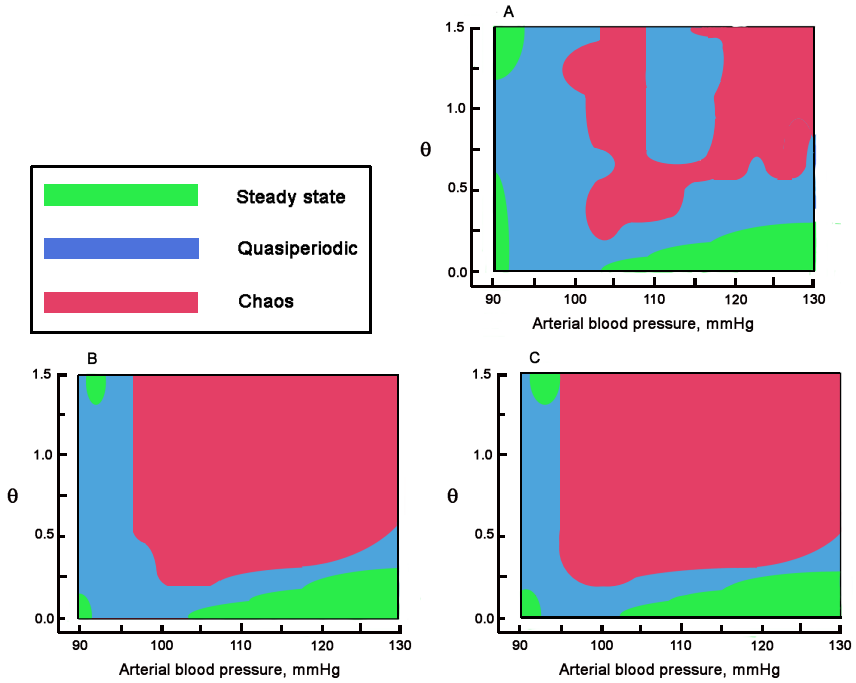

Figure 4.29: Dynamical behavior regimes as a function of arterial pressure and θ, the strength of nephron nephron coupling. (a): nephron 1, the most superficial cortical nephron; (b): nephron 15, the shortest juxtamedullary nephron; and (c): nephron 22, the longest juxtamedullary nephron.

In all cases these nephron simulations retain a strong component at the TGF frequency. As can be seen in all panels the complete absence of nephron-nephron communication generates oscillations over a range of arterial pressures from 93 to 103 $mmHg$. On both sides of this interval the model generates steady state behavior for all nephrons. The arterial pressure is here either too low or too

high for the TGF regulation to be active, and the nephrons operate in one of the saturation regimes for the S-shaped curve determining the activation of the arteriole smooth muscles Ψ. Quasiperiodicity appears over intermediate ranges of θ and arterial pressure for all nephrons. The fraction of the plane covered by quasiperiodic behavior is maximal in nephron 1 and diminishes in deeper and longer nephrons. For the rest there are trajectories that form strange attractors on the phase plane.

The simulations in Fig. 4.29a represent the behavior of the most superficial cortical nephrons from which the available experimental results have been collected. In animal experiments the arterial pressure is easily changed, but the value of θ is not. The value of this parameter is in the range 0.25–0.5 in normal animals (Chen et al., 1995; Wagner et al., 1997). As mentioned above, oscillations in tubular pressure are typically measured in normal rats over the arterial pressure range 95–130 $mmHg$. Fig. 4.29a shows a region of chaotic behavior in the arterial pressure range 100–115 $mmHg$ when θ lies between 0.25 and 0.5. Results such as these have not been reported in animal experiments that have concentrated precisely in this area of the parameter plane. We address possible sources of this discrepancy in Discussion.

Chapter 5

Discussion

5.1 Interaction between regulatory mechanisms

Nonlinear interactions between TGF and the myogenic mechanism are probably important signaling mechanisms in renal autoregulation. The two different forms of modulation we have presented, both of which arise from nonlinear interactions, solve two different problems:

- The first is time coordination and stabilization. The arterial pressure can change rapidly. Propagation of a pressure disturbance through the tubular system to the macula densa entails a delay of 10–15 s. The myogenic mechanism can respond to the same signal in a fraction of this time. Unless there is some way to coordinate the two mechanisms they could act in an uncoordinated manner, and fail to provide adequate autoregulation. Amplitude modulation should permit the actions of the two mechanisms to act cooperatively. In manmade control systems, the introduction of a fast, low ampltidude signal inside the feedback loop of a nonlinear controller has the effect of narrowing the nonlinear sector and stabilizing the system (Zames and Schneyder, 1977). Because TGF is a nonlinear system, its interaction with the myogenic mechanism improves the stability of autoregulation. When the blood pressure increases, the kidney needs the afferent arteriolar resistance to increase, and vice versa. Without some form of coordination between the two mechanisms it is to be expected that

the system would fail to respond as the kidney needs it to, and that the blood flow will fluctuate inappropriately. Amplitude modulation helps to prevent this.

- Frequency modulation solves a second problem, which is the fidelity of signal transmission. Frequency modulation is well known in signal processing as a robust method for sending and receiving signals in a noisy environment. Arteriolar smooth muscle contraction is triggered by increasing Ca, but Ca has many more functions in these cells than controlling muscle contraction. It is no exaggeration to say that the Ca environment of these cells is noisy. Spatial inhomogeneity is one answer to this problem, and recent evidence points to localization of calmodulin with voltage gated Ca channels which are inhomogeneously distributed in the plasma membrane (Mori et al., 2004). Frequency modulation is another, complementary way to connect the signal and the target.

5.2 Nephron-to-nephron communication

The relative strengths of the two coupling mechanisms depends on the structure of the arteriolar network. While the hemodynamic coupling primarily depends on the length and diameter of the shared interlobular artery in comparison with the lengths and diameters of the separated arterioles, the vascular coupling depends on the propagation distance for the TGF response relative to a characteristic decay length for this response. Because of its instantaneous character, the vascular response tends to produce in-phase synchronization between the neighboring nephrons. The hemodynamic coupling, on the other hand, involves a delay and, hence, tends to produce out-of-phase or anti-phase synchronization. The result that most of the available experiments show in-phase synchronization is associated with the fact that we have selected nephrons that are situated close to one another. The single example of anti-phase synchronization observed so far was obtained for a couple of nephrons that were placed too far from one another for the vascular coupling to be active. It has been shown that 60–70%

of all nephrons are organized in couples or triplets (Källskog and Marsh, 1990). Moreover, the average lengths of the vascular segments separating neighboring glomeruli have been measured to be 250–300 μm. This is only about 30% of the length that a vascular signal is expected to propagate, suggesting that a large fraction of the nephrons may act in groups rather than as independent functional units.

We evaluated synchronization phenomena in interacting nephrons by measuring both frequency and phase synchronization. Statistical analysis showed that synchronization among mechanisms of renal autoregulation is reduced in hypertensive rats. Normotensive rats demonstrate full entrainment in which both oscillatory modes, associated with two mechamisms of autoregulation, are synchronized; the probability in both tests exceeds 70%. Spontaneously hypertensive rats generally were in a synchronous state for only 1/3 to 1/2 as long as the normotensive ones; they have about half the probability of full synchronization and about twice the probability of partial synchronization where neighbouring nephrons attain a state of synchronization with respect to their slow tubuloglomerular feedback dynamics, but the fast myogenic dynamics remain desynchronized, or vice versa.

We suggest that the less frequent synchronization we found in SHR could have at least two sets of functional consequences:

- First, consider the effects on blood flow distribution. We recently simulated the interactions among oscillating nephrons of different lengths supplied by a single cortical radial artery that could be synchronized by vascular signals. With no vascular coupling the simulation showed that the fraction of cortical radial artery blood flow received by each nephron varied with time because the oscillations were not synchronized. Vascular coupling produced synchronization of nephrons and an oscillation of mean vascular pressure in the cortical radial artery, and the fractional delivery of blood to each nephron remained constant throughout the TGF cycle. The results of this study suggest that because of decreased synchronization, fractional blood flow distribution among nephrons of SHR

will be more highly variable, an effect that could cause more highly variable GFR. Episodes of elevated glomerular filtration rate (GFR) from this source could contribute to impaired regulation of solute excretion and to glomerular damage.

- A second consequence of imperfect synchronization among nephrons will likely be irregular delivery of tubular fluid to distal nephron segments. We have found oscillations in distal tubule pressure and of distal tubule Cl concentration at the TGF frequency, indicating that fluid delivery to distal segments retains some of the dynamic properties of nephron blood flow and GFR. Cortical collecting tubules and inner medullary collecting ducts receive tubular fluid from a number of nephrons. It is likely that the dynamics of fluid delivery to these tubular junctions will depend on the dynamics of blood flow and GFR regulation; if nephron blood flows are synchronized so too will be distal delivery. Non-coherent blood flow regulation among nephrons is likely to cause non-coherent delivery into collecting tubules and ducts. At stake here are flow dependent K secretion and hormone dependent reabsorption of Na, Cl, and other ions. Modern understanding of these processes is described only as if the flows remain steady in time. The steady state formulation is equivalent to an assumption that flow rates in all distal tubules feeding a cortical collecting duct are synchronized. In the absence of synchronization, or if synchronization is intermittent, flow and solute load dependent processes may not generate time average values equivalent to tubules operating in a steady state. It remains to be seen whether these effects, if they do occur, have functional consequences.

5.3 Modelling approach

We simulated the dynamical behavior of a group of nephrons that derive their blood supply from a single cortical radial artery in a rat kidney. The simulations include simplified representations of the adaptive mechanisms present in every

nephron that regulate blood flow. The cortical radial artery is an example of a resource distribution network (Postnov et al., 2005). All the blood flowing into it is distributed to the nephrons whose arterioles branch from it, with none remaining at the end. The cortical radial artery is relatively large compared to the arterioles, and we assumed that active control of blood flow is exercised by the nephrons, and none by the artery. In addition to local regulation of blood flow, nephrons communicate with each other by sending electrical signals over the vascular wall. The signals are initiated by TGF, the mechanism that provides local regulation of blood flow, and influences the vascular response of adjacent nephrons (Holstein-Rathlou, 1987; Källskog and Marsh 1990; Chen et al., 1995; Wagner et al., 1997).

We used the simulation to address several questions:

- First, is nephron-to-nephron communication sufficient to explain the strong synchronization of tubular pressure oscillations found in normal rats and those with hypertension (Holstein-Rathlou, 1987; Yip et al., 1991; Yip et al., 1992). In the simulation all of the short cortical nephrons synchronize at a single frequency, even when the time delays in the TGF loop are made to vary randomly, and also when the cortical nephrons operate in a chaotic domain. The longer medullary nephrons consistently form two different clusters each operating at a unique frequency, and neither synchronizing with the cortical nephrons.

- What is the relative significance of different coupling mechanisms? Two types of nephron-to-nephron communication have been discussed: by electrical signalling over the vascular wall, and by modifying the local hydrostatic pressure in the cortical radial artery, called hemodynamic coupling (Moore et al., 1992; Postnov et al., 2005). Hemodynamic coupling predicts out of phase oscillations in adjacent nephrons, but it can only be effective if the contraction of a single afferent arteriole can make an appreciable difference in the vascular pressure. Our simulation results show that adjacent cortical nephrons oscillate at a single frequency and with small phase angle differences. The possibility of this type of synchronization was pre-

dicted by our model and subsequently found in the experiments. The effect of electrical coupling over the vascular wall overwhelms the possible effect of hemodynamic coupling.

- The third question relates to the limitations of the present model. TGF provides an S-shaped Ψ response to flow in the loop of Henle, and direct measurements show that the mechanism saturates at either high or low flow rates with a narrow range of pressures over which effective regulation is possible. This result is not consistent with other experimental results; higher arterial pressures generate larger oscillations (Yip et al., 1993). Two explanations for this discrepancy come to mind: coupling within the nephron ensemble is responsible, or the model is too simple. A more detailed nephron model, which has a spatially distributed renal tubule, and a contractile mechanism in afferent arteriolar cells shows oscillations in both TGF and the myogenic mechanism, and the amplitudes of the oscillations increase monotonically with arterial pressure over the range 95 – 130 $mmHg$ (Marsh et al., 2005). At higher arterial pressures and higher values of coupling strength each of the nephrons in the ensemble is capable of a bifurcation to chaos. The simulation suggests that the nephron ensemble instability increases at higher arterial pressures and values of the coupling strength, which occurs when blood pressure elevations become chronic.

Bibliography

Ashcroft FM and Rorsman P (1989) Electrophysiology of the pancreatic β-cell. Prog Biophys Mol Biol 54: 87–143.

Alpern RJ and Heber SC (2008) Seldin and Giebisch's the kidney: Physiology and pathophysiology. 4th edition Elsevier Academic Press.

Anishchenko VS (1995) Dynamical chaos—models and experiments. Singapore, World Scientific.

Barfred M, Mosekilde E, Holstein-Rathlou N-H (1996) Bifurcation analysis of nephron pressure and flow regulation. Chaos 6: 280–287.

Bell PD, Lapointe JY, Peti-Peterdi J (2003) Macula densa cell signaling. Annu Rev Physiol 65: 481–500.

Bertau M, Mosekilde E, Westerhoff (2008) Biosimulation in Drug Development. Wiley, Weinheim.

Blinowska K and Marsh D (1985) Ultra- and circadian fluctuations in arterial pressure and electromyogram in conscious dogs. Am J Physiol 249: R720–R725.

Braun HA, Wissing H, Schfer K, Hirsch MC (1994) Oscillation and noise determine signal transduction in shark multimodal sensory cells. Nature 367: 270–273.

Casellas D, Bouriquet N, Moore LC (1997) Branching patterns and autoregulatory responses of juxtamedullary afferent arterioles. Am J Physiol 272: F416–421.

Casellas D, Dupont M, Bouriquet N, Moore LC, Artuso A, Mimran A (1994) Anatomic Pairing of Afferent Arterioles and Renin Cell Distribution in Rat Kidneys. Am J Physiol 267: F931–F936.

Casellas D and Moore LC (1990) Autoregulation and tubuloglomerular feedback

in juxtamedullary glomerular arterioles. Am J Physiol 258: F660–F669.

Cannon WB (1929) Organization for physiological homeostasis. Physiol Rev 9: 399–431.

Chen YM, Yip KP, Marsh DJ, Holstein-Rathlou N-H (1995) Magnitude of TGF-initiated nephron-nephron interactions is increased in SHR. Am J Physiol 269 (Renal Fluid Electrolyte Physiology 38): F198–204.

Chon KH, Chen YM, Marmarelis VZ, Marsh DJ, Holstein-Rathlou N-H (1994) Detection of interactions between myogenic and TGF mechanisms using nonlinear analysis. Am J Physiol Renal Physiol 267: F160–F173.

Chon KH, Raghavan R, Chen YM, Marsh DJ, Yip KP (2005) Interactions of TGF-dependent and myogenic oscillations in tubular pressure. Am J Physiol Renal Physiol 288: F298–F307.

Clausen G, Oien AH, Aukland K (1992) Myogenic vasoconstriction in the rat kidney elicited by reducing perirenal pressure. Acta Physiol Scand 144: 277–290.

Colantuoni A, Bertuglia S, Intaglietta M (1984) Quantification of rhythmic changes in the arterial microcirculation. Am J Physiol 246: H508–H517.

Daubechies I (1992) Ten lectures on wavelets. S.I.A.M., Philadelphia.

Davis MJ and Hill MA (1999) Signaling mechanisms underlying the vascular myogenic response. Physiol Rev 79: 387–423.

Deen WM, Robertson CR, Brenner BM (1984) A model of glomerular ultrafiltration in the rat. Am J Physiol 223: 1178–1183.

di Rienzo M, Castiglioni P, Mancia G, Parati GG, Pedotti A (1989) 24 h sequential spectral analysis of arterial blood pressure and pulse interval in free-moving subjects. IEEE Trans Biomed Eng 36: 1066–1075.

Gabor D (1946) Theory of communication. J. IEE (London) 93: 429–457.

Glass L and Mackey MC (1988) From clocks to chaos: The rhythms of life. Princeton University Press, Princeton.

Goldbeter A (1996) Biochemical oscillations and cellular rhythms. Cambridge University Press, Cambridge.

Grossman A and Morlet J (1984) Decomposition of Hardy functions into square

integrable wavelets of constant shape. SIAM J Math Anal 15: 723–736.

Hayashi C (1964) Nonlinear oscillations in physical systems. McGraw-Hill, New York.

Hoffman U, Yanar A, Franzeck UK, Edvards JM, Bollinger A (1990) The frequency histograma new method for the evaluation of laser Doppler flux motion. Microvascular Res 40: 293–301.

Holstein-Rathlou N-H (1987) Synchronization of proximal intratubular pressure oscillation: Evidence for interaction between nephrons. Pflügers Arch 408: 438–443.

Holstein-Rathlou N-H, He J, Wagner AJ, Marsh DJ (1995) Patterns of blood pressure variability in normotensive and hypertensive rats. Am J Physiol 269 (Regulatory Integrative Comparative Physiol 38): F1230–F1239.

Holstein-Rathlou N-H and Leyssac PP (1986) TGF-mediated oscillations in the proximal intratubular pressure: differences between spontaneously hypertensive rats and Wistar-Kyoto rats. Acta Physiol Scand 126: 333–339.

Holstein-Rathlou N-H and Leyssac PP (1987) Oscillations in the proximal intratubular pressure: a mathematical model. Am J Physiol 252 (Renal Fluid Electrolyte Physiol. 21): F560–F572.

Holstein-Rathlou N-H and Marsh DJ (1989) Oscillations of tubular pressure, flow, anddistal chloride concentrations in rats. Am J Physiol 256: F1007–F1014.

Holstein-Rathlou N-H and Marsh DJ (1990) A dynamic model of the tubuloglomerular feedback mechanism, Am J Physiol 258: F1448–F1459.

Holstein-Rathlou N-H, Wagner AJ, Marsh DJ (1991) Tubuloglomerular feedback dynamics and renal blood flow autoregulation in rats. Am J Physiol 260: F53–68.

Holstein-Rathlou N-H, Yip KP, Sosnovtseva OV, Mosekilde E (2001) Synchonization phenomena in nephron-nephron interaction. Chaos 11: 417–426.

Jensen KS, Mosekilde E, Holstein-Rathlou N-H (1986) Self-sustained oscillations and chaotic behavior in kidney pressure regulation. Mondes Development 54/55: 91–109.

Johnson PC (1980) The myogenic response, in Handbook of Physiology, Volume

II: Vascular smooth muscle, Section 2: The Cardiovascular system, edit. by D.F. Bohr, A.P. Somlyo, H.V. Sparks, and Jr. M.D. Bethesda. American Physiologycal Society: 409–442.

Just A (2007) Mechanisms of renal blood flow autoregulation: dynamics and contributions. Am J Physiol Regul Integr Comp Physiol 292: R1–R17.

Just A, Wittmann U, Ehmke H, Kirchheim HR (1998) Autoregulation of renal blood flow in the conscious dog and the contribution of the tubuloglomerular feedback. J Physiol 506: 275–290.

Kaiser G (1994) A friendly guide to wavelets. Boston, Birkhäuser.

Kantz H and Schreiber T (2004) Nonlinear time series analysis. Cambridge University Press, Cambridge.

Kopell N, Ermentrout GB, Whittington MA, Traub RD (2000) Gamma rhythms and beta rhythms have different synchronization properties . Proc Natl Acad Sci USA 97: 1867–1872.

Kuznetsov PI, Stratonovich RL, Tikhonov VI (1965) Non-linear transformation of stochastic process. Pergamon, Oxford.

Källskog, Ö and Marsh DJ (1990) TGF-initiated vascular interactions between adjacent nephrons in the rat kidney. Am J Physiol 259 (Renal Fluid Electrolyte physiol 28): F60–F64.

Landa PS (1980) Self-oscillations in the systems with a finite number of degrees of freedom. Nauka, Moscow (in Russian).

Leng G (1988) Pulsatility in neuroendocrine systems. CRC Press, Boca Raton, FL.

Leyssac PP and Baumbach L (1983) An oscillating intratubular pressure response to alterations in the loop of Henle flow in the rat kidney. Acta Physiol Scand 117: 415–419.

Leyssac PP and Holstein-Rathlou N-H (1989) Tubulo-glomerular feedback response: enhancement in adult spontaneously hypertensive rats and effect of anaesthetics. Pflügers Arch 413: 267–272.

Loutzenhiser R, Bidani A, Chilton L (2002) Renal myogenic response: kinetic attributes and physiological role. Circ Res 90: 1316–1324.

Mallat SG (1998) A wavelet tour of signal processing. San Diego, Academic Press.

Marcus FB (2008) Bioinformatics and systems biology: Collaborative research and resources. Springer.

Marsh DJ, Osborn JL, A.W. Cowley AW Jr (1990) 1/f fluctuations in arterial pressure and the regulation of renal blood flow in dogs. Am J Physiol 258 (Renal Fluid Electrolyte Physiol. 27): F1394–F1400.

Marsh DJ, Sosnovtseva OV, Pavlov AN, Yip KP, Holstein-Rathlou N-H (2005) Frequency encoding in renal blood flow regulation. Am J Physiol Reg Integ Comp Physiol 288: R1160–R1167.

Meyer Y (1992) Wavelets and applications. Springer-Verlag, Berlin.

Moore LC and Casellas D (1990) Tubuloglomerular feedback dependence of autoregulation in juxtamedullary afferent arterioles, Kidney Int 37: 1402–1408.

Moore LC, Rich A, Casellas D (1992) Ascending myogenic autoregulation: Interactions between tubuloglomerular feedback and myogenic mechanisms. Bull Math Biol 56: 391–410.

Mori MX, Erickson MG, Yue DT (2004) Functional stoichiometry and local enrichment of calmodulin interacting with Ca_i^{2+} channels. Science 304: 432–435.

Mosekilde E (1996) Topics in nonlinear dynamics: Applications to physics, biology and economic Systems World Scientific, Singapore.

Mosekilde E, Sosnovtseva OV, Holstein-Rathlou N-H (2005) Mechanism-based modeling of complex biomedical systems. Basic & Clinical Pharmacology & Toxicology 96: 212–224.

Muzy JF, Bacry E, Arneodo A. (1994) The multifractal formalism revisited with wavelets. Int J Bifurcation Chaos 4: 245–302.

Müller-Suur R, Ulfendahl HR, Persson AE (1983) Evidence for tubuloglomerular feedback in juxtamedullary nephrons of young rats. Am J Physiol Renal Physiol 244: F425–F431.

Nicolis C and Prigogine I (1977) Self-organization in nonequilibrium systems. Wiley, New York.

Nordsletten LC, Blackett S, Bentley MD, Ritman EL, Smith NP (2006) Structural morphology of renal vasculature. Am J Physiol Heart Circ 291: H296–309.

Pavlov AN, Sosnovtseva OV, Pavlova ON, Mosekilde E, Holstein-Rathlou N-H (2008) Characterizing multimode interaction in renal autoregulation. Physiol Meas 29: 945–958.

Peng C-K, Havlin S, Stanley HE, Goldberger AL (1995) Quantification of scaling exponents and crossover phenomena in nonstationary heartbeat time series. Chaos 5: 82–87.

Rettig R, Folberth C, Stauss H, Kopf D, Waldherr R, Unger T (1990) Role of the kidney in primary hypertension: a renal transplantation study in rats. Am J Physiol Renal Physiol 258: F606–F611.

Rettig R, Stauss H, Folberth C, Ganten D, Waldherr B, Unger T (1989) Hypertension transmitted by kidneys from stroke-prone spontaneously hypertensive rats. Am J Physiol Renal Physiol 257: F197–F203.

Pires SL, Barres C, Sassard J, Julien C (2001) Renal blood flow dynamics and arterial pressure lability in the conscious rat. Hypertension 38: 147–152.

Pitman BE, Zaritski RM, Kesseler KJ, Moore LC, Layton HE (2004) Feedback-mediated dynamics in two coupled nephrons. Bull Math Biol 66: 1463–1492.

Postnov DE, Sosnovtseva OV, Mosekilde E (2005) Oscillator clustering in a resource distribution chain. Chaos 15: 13704(1-12).

Schnermann J and Briggs JP (1989) Interaction between loop of Henle flow and arterial pressure as determinants of glomerular pressure. Am J Physiol 256: F421–F429.

Schnermann J and Levine DZ (2003) Paracrine factors in tubuloglomerular feedback: adenosine, ATP, and nitric oxide. Annu Rev Physiol 65: 501–529.

Schnermann J, Traynor T, Yang T, Arend L, Huang YG, Smart A, Briggs JP (1998) Tubuloglomerular feedback: new concepts and developments. Kidney Int Suppl 67: S40–S45.

Schubert R and Mulvany MJ (1999) The myogenic response: established facts and attractive hypotheses. Clin Sci (Lond) 96: 313–326.

Sjöquist M, Göransson A, Källskog O, Ulfendahl HR (1984) The influence of tubulo-glomerular feedback on the autoregulation of filtration rate in superficial and deep glomeruli. Acta Physiol Scand 122: 235-242.

Schäfer C, Rosenblum MG, Kurths J, Abel H-H (1998) Heartbeat synchronized with ventilation. Nature (London) 392: 239–240.

Smedley GT, Yip KP, Wagner AJ, Dubovitsky S, Marsh DJ (1993) A laser Doppler velocimetry instrument for in-vivo measurements of blood flow in single renal arterioles. IEEE Trans Biomed Eng 40: 290–297.

Sosnovtseva OV, Pavlov AN, Mosekilde E, Holstein-Rathlou N-H (2002a) Bimodal oscillations in nephron autoregulation. Phys Rev E 66: 1–7.

Sosnovtseva OV, Pavlov AN, Mosekilde E, Holstein-Rathlou N-H, Marsh DJ (2004) A double-wavelet approach to study frequency and amplitude modulation in renal autoregulation. Phys Rev E 70: 031915.

Sosnovtseva OV, Postnov DE, Nekrasov AM, Mosekilde E, Holstein-Rathlou N-H (2002b) Phase multistability analysis of self-modulated oscillations. Phys Rev E 66: 036224.

Stratonovich LR (1963) Topics in the theory of random noise. Gordon and Breach, New York.

Thomas SR, Layton AT, Layton HE, Moore LC (2006) Kidney modelling: status and perspectives. Proceedings of the IEEE 94: 740–752.

Thomson SC and Blantz RC (1988) Tubuloglomerular feedback. Am J Nephrol 8: 393–401.

van der Pol B (1927) Forced oscillations in a circuit with non-linear resistance. Phil Mag 3: 65–80.

Wagner AJ, Holstein-Rathlou N-H, Marsh DJ (1997) Internephron coupling by conducted vasomotor responses in normotensive and spontaneously hypertensive rats. Am J Physiol 272 (Renal Physiol 41): F372–F379.

Wang H, Kin S, Ju K, Chon KH (2006) A high resolution approach to estimating time-frequency spectra and their amplitudes. Ann Biomed Eng 34: 326–338.

Wang X-J and Rinzel J (1995) in The Handbook of Brain Theory and Neural Networks ed. M.A. Arbib MIT Press, Cambridge.

Wolf MM, Varigos GA, Hunt D, Sloman JG (1978) Sinus arrhythmia in acute myocardial infarction. Med J Australia 2: 52–53.

Wronski T, Seeliger E, Persson PB, Forner C, Fichtner C, Scheller J, Flemming B

(2003) The step response: a method to characterize mechanisms of renal blood flow autoregulation. Am J Physiol Renal Physiol 285: F758–F764.

Yip KP, Holstein-Rathlou N-H, Marsh DJ (1991) Chaos in blood flow control in genetic and renovascular hypertensive rats. Am J Physiol 261: F400–408.

Yip KP, Holstein-Rathlou N-H, Marsh DJ (1992) Dynamics of TGF-initiated nephron-nephron interactions in normotensive rats and SHR. Am J Physiol 262 (Renal Fluid Electrolyte Physiol 31): F980–F988.

Yip KP, Holstein-Rathlou N-H, Marsh DJ (1993) Mechanisms of temporal variation in single-nephron blood flow. Am J Physiol 264: F427–434.

Yip KP, Marsh DJ, Holstein-Rathlou N-H (1995) Low dimensional chaos in renal blood flow control in genetic and experimental hypertension. Physica D 80: 95–104.

Zames G and Schneyder NA (1977) Structural stabilization and quenching by dither in nonlinear systems. IEEE Trans Automatic Control 22: 352–361.

Verzeichnis der akademischen Lehrer

Meine akademischen Lehrer waren Damen/Herren

... in Marburg

Braun, Huber, Voigt, Schneider

... in Berlin

Kurths, Pikovsky, Rosenblum, Schimansky-Geir, Zaks

... in Copenhagen

Abdali, Holstein-Rathlou, Knudsen, Mosekilde

... in Brown

Marsh

... in Saratov

Anischenko, Astahov, Bezruchko, Hohlov, Neiman, Postnov, Salij, Trubetskov, Tuchin, Vadivasova, Usanov

... in Mirnyj

Gavrilova, Harlamova, Kapralova, Matveeva, Nikolaeva, Sidorova, Sledova, Potapova, Rastyagaeva

Danksagung

I am deeply indebted to **Prof. Niels-Henrik Holstein-Rathlou**, Head of the Department of Biomedical Sciences, Copenhagen University, and **Prof. Donald Marsh**, Brown University, USA, for introducing me to the filed of renal physiology, for sharing with me their experience and ideas, for their guidance throughout my research, and for their active support. Without these two people this work would not have been done.

I would like to thank my supervisor **Dr. Hans Braun** for his support of my wish to study physiology and get PhD degree based on the research in interdisciplinary field. I thank my other supervisor **Prof. Karlheinz Voigt** for his encouragement and advices throughout my work.

I want to express my sincere gratitude to **Prof. Erik Mosekilde** for fruitful collaboration over time and space scales. I appreciate very much invaluable scientific experience which I gained by working together in the filed of nonlinear dynamics and systems biology.

Prof. Dmitry Postnov and **Dr. Alexey Pavlov** provided important contributions to the present work. I thank them for the helpful and enjoyable collaboration throughout many years.

I thank all my **academic teachers** from Saratov State University for the knowledge they gave me. I wish to acknowledge my friends and colleagues **Dr. Nadezda Brazhe, Dr. Alexey Brazhe** and **Prof. George Maksimov** for support and collaboration on other related projects. I thank all my colleagues in Germany, England and USA for their support, advices and helpful discussions.

I gratefully acknowledge the help of **Svetlana Postnova** with official documents related to thesis submission.

Finally I want to express my gratitude to **my family** for their patience and continuing support.